The neurophysiology of closed-loop auditory stimulation in sleep: a MEG study

Hugo R. Jourde[1-4], Raphaëlle Merlo[5], Mary Brooks[1], Meredith Rowe[6], and Emily B.J. Coffey[1-4,6]✉

[1]Concordia University, Montreal, Canada
[2]International Laboratory for Brain, Music and Sound Research (BRAMS)
[3]Centre for Research on Brain, Language and Music (CRBLM)
[4]Quebec Bio-Imaging Network (QBIN)
[5]Université de Montréal, Montreal, Canada
[6]McGill University, Montreal, Canada

Closed-loop auditory stimulation (CLAS) is a brain modulation technique in which sounds are timed to enhance or disrupt endogenous neurophysiological events. CLAS of slow oscillation up-states in sleep is becoming a popular tool to study and potentially enhance sleep's functions, as it can increase slow oscillations, evoke sleep spindles, and enhance memory consolidation of certain tasks. However, few studies have examined the specific neurophysiological mechanisms involved in CLAS, in part because of practical limitations to commonly-used tools. To evaluate evidence for possible models of how sound stimulation during brain up-states might generate slow oscillations, we simultaneously recorded electro- and magnetoencephalography in human participants who received auditory stimulation across sleep stages and neural oscillation phases. The results suggest that auditory information reaches ventral frontal lobe areas via non-lemniscal pathways. From there, a slow oscillation is created and propagated. We demonstrate that while the state of excitability of tissue in auditory cortex and frontal ventral regions shows some synchrony with the EEG-recorded up-states that are commonly used for CLAS, it is the state of ventral frontal regions that is most critical for slow oscillation generation. Our findings advance models of how CLAS leads to enhancement of slow oscillations, sleep spindles, and associated cognitive benefits, and offer insight into how the effectiveness of brain stimulation techniques can be improved.

sleep | closed-loop stimulation | sleep stages | auditory evoked response | electroencephalography (EEG) | magnetoencephalography (MEG) | sleep spindles | slow oscillations

Correspondence: ***emily.coffey@concordia.ca***

Introduction

Closed-loop brain stimulation is a technique in which sensory, magnetic or electric stimulation is timed to modulate endogenous brain activity or states (see Antony et al. (2022) for a discussion of terminology). Its main appeal to neuroscientists is the ability to test relationships between brain activity and function causally, thus adducing strong evidence for the roles of neural events and processes. Closed-loop auditory stimulation (CLAS) of slow oscillations during non-rapid eye movement (NREM) sleep has enjoyed particular attention, perhaps due to the unique (and still somewhat mysterious (Girardeau and Lopes-Dos-Santos, 2021)) physiological processes that take place in sleep.

Sleep is a collection of neurophysiological states with several crucial functions including cleaning waste produced during wakeful activity (Hauglund et al., 2020), rescaling synapses (Blanco et al., 2015, Timofeev and Chauvette, 2017), and transforming temporarily-stored memories into lasting ones in a process known as memory consolidation (Antony et al., 2019, Diekelmann and Born, 2010, Klinzing et al., 2019, Schabus et al., 2004). These processes seem to rely on sleep-specific neurophysiological events that are most often measured in EEG: slow oscillations, K-complexes (also referred to as 'N550-P900 complexes' when evoked by external stimuli), and sleep spindles. Slow oscillations (SOs) refer to low frequency brain activity that is defined variously as $<$1.0, 1.5, 2, or 4 Hz (Carrier et al., 2011, Jaar et al., 2010, Ngo et al., 2013, Vyazovskiy and Harris, 2013). These high-amplitude fluctuations in cortical and subcortical excitability occur during NREM sleep (stages N2 and N3) and appear to be involved in all three processes (Hauglund et al., 2020, Klinzing et al., 2019, Neske, 2016, Timofeev and Chauvette, 2017). N550-P900 complexes are a particular kind of evoked slow oscillation that also occur during stage N2 and N3 sleep (about 550 to 900 ms after sensory input) (Bellesi et al., 2014, Latreille et al., 2020, Riedner et al., 2011). They are highly related to and

often considered to be K-complexes, although K-complexes can be generated in the absence of external stimulation. N550-P900 complexes have been linked to sleep continuity and arousal (Halász, 2016). Sleep spindles are transient (<2.5 s) 11-16 Hz bursts of activity that are generated through thalamocortical interactions. They frequently co-occur with slow oscillations, may be evoked by sensory stimulation (Sato et al., 2007), and are linked to memory and consolidation processes (see Fernandez and Lüthi (2020) for a comprehensive review).

Closed-loop auditory stimulation of slow oscillations, and subsequent enhancement of memory consolidation of performance on a declarative memory task (e.g. word list learning), was first reported by Ngo et al. (2013). CLAS of SOs has since been repeatedly used in sleep research due to its convenience, ease of use, and temporal precision (see recent reviews Choi et al. (2020), Harrington and Cairney (2021)). As with other forms of brain stimulation, effectiveness can vary considerably across subjects (Nasr et al., 2022). Timing of stimulation seems crucial, and stimulation close to SO peaks (i.e., the 'up-state') best enhances sleep-related memory consolidation processes (Navarrete et al., 2020). Stimulation during the trough (i.e., the 'down-state') can result in a decrease in spindle activity and delta power (Moreira et al., 2021, Ngo et al., 2013). The SO up-states (measured as peaks in EEG) are thought to represent a state of higher excitability of cortical tissues which are thus closer to their firing thresholds, meaning they are more readily activated upon auditory stimulation. It is thought to be through evoked neural events that memory consolidation is enhanced (Bellesi et al., 2014); however, the neurophysiological mechanisms underlying the effects of CLAS to slow oscillation up-states are poorly understood.

Evoked brain responses (i.e., event-related potentials in electroencephalograpy; ERPs) are used in sleep research to characterize the evolution of sensory processing according to the depth of sleep (reviewed in Colrain and Campbell (2007)). The amplitude and latency of typical patterns of peaks and troughs, sometimes called 'components', are somewhat affected by deepening sleep stage (Niiyama et al., 1994, Ogilvie et al., 1991). The N100 component (i.e., a negative peak occurring about 100 ms after sound onset), is often reported to be attenuated during sleep, whereas P200 (i.e., a positive peak about 200 ms after onset) increases in deeper sleep (Campbell et al., 2010). Some evoked components occurring more than 300 ms after stimulation only appear during sleep (Bastien et al., 2002). Three of these components, labelled N350, N550 and P900 (i.e., negative deflections occurring at about 350 and 550 ms and a positive deflection at about 900 ms post onset) begin to emerge at NREM sleep onset (stage N1) and their amplitude increases with sleep depth (stages N2 and N3). The N550-P900 complex has an asymmetrical shape composed of a trough in which cortical neurons are hyperpolarized, followed by a longer rebound of cortical activity during which neurons are comparatively depolarized and thus more excitable (Latreille et al., 2020). Recent work using electrical source localization models suggests that the spontaneous K-complex, which is similar to the sensory-evoked N550-P900 complex (Halász, 2016), originates in ventral limbic cortex, including medial temporal and caudal orbitofrontal cortex (OFC) (Morgan et al., 2021).

Because the specific auditory pathway involved in closed-loop auditory stimulation is not yet well understood, we must consider the anatomy of the auditory system. There are two main ascending auditory pathways: the lemniscal or primary pathway, and the non-lemniscal or secondary pathway. In the lemniscal pathway, the primary auditory cortex receives projections from the cochlear nucleus via the central nucleus of the inferior colliculus (IC) and the ventral division of the medial geniculate body of the thalamus (MGB). The non-lemniscal pathway consists of many sets of fibres that send and receive feed-forward and feedback projections widely in midbrain, cortical and limbic areas (Lee, 2015). Of interest here are fibres originating in the brainstem which project to the dorsal division of the medial geniculate body of the thalamus and to secondary auditory cortex, and those which interact with the ascending reticular activating system (ARAS). The ARAS is comprised of many nuclei with connections to the rest of the cortex (Yeo et al., 2013). It also has connections to the locus coeruleus (LC), a group of large nuclei in the brainstem (Bellesi et al., 2014, Poe et al., 2020). The LC is the principal source of norepinephrine/noradrenaline in the brain and has widespread (though sparse) projections to the cortex. Both the LC and ARAS are involved in transitioning among arousal states, meaning that there is overlap between the auditory non-lemsniscal pathways and the arousal-promoting systems (Bellesi et al., 2014, Wijdicks, 2019).

Evidence suggests that elements of the auditory system, as well as general arousal mechanisms that are independent of the auditory modality (Riedner et al., 2011), are involved in generating the slow oscillations observed in the CLAS effect (Bellesi et al., 2014). However; how, where, and when these systems conspire to produce SOs is unknown, and their contributions to

the more commonly-studied cortical EEG evoked responses are not yet understood. Next, we define four possible variations on models of auditory-arousal system interactions. Each leads to different predictions in the location, amplitude, and timing of evoked responses to sound in NREM sleep, which can be assessed with temporally- and spatially-resolved neuroimaging methods.

The four models, which vary in the timing and involvement of arousal networks and the location of initial SO generation, are illustrated in Figure 1. In the first model, auditory sensory information reaches the auditory cortex (AC) through lemniscal auditory pathways, where it generates a slow oscillation that propagates locally. In this case, only the auditory cortex should exhibit early auditory evoked components (P100, N100, P200), and in NREM sleep, the evoked slow oscillations should occur earlier and with high amplitude in auditory cortex as compared with other regions. In the second model, auditory information reaches auditory cortex as above, but then propagates to other cortical regions including frontal areas via structural connections (see Plakke and Romanski (2014)). Upon arrival in the ventral frontal regions, the neural impulse induces a slow oscillation locally, due to regional differences in the propensity for SO generation (Massimini et al., 2004). In this case, the auditory cortex is not the primary generator of evoked slow oscillations, but the process of SO generation is dependent upon a robust response in the auditory cortex. This model would predict the absence of auditory response in the OFC (orbitofrontal cortex), and that late components would appear first and strongest in ventral frontal regions (like OFC), and then later in other cortical regions. In the third model, as auditory information travels simultaneously through the lemniscal and non-lemniscal pathways, non-lemniscal neurons interact with arousal systems in the brainstem (possibly involving LC) and/or thalamus, which then result in diffuse changes in cortical excitability, leading to the generation of slow oscillations throughout the brain. An early auditory-like response and then stronger, later responses in the OFC then might be expected due to the previously-observed tendency for ventral limbic areas (including OFC) to generate endogenous slow oscillations (Massimini et al., 2004, Morgan et al., 2021). The fourth model is a modification of the third model, in which auditory information primarily generates the CLAS effect via the non-lemniscal auditory pathway. The impulse would preferentially stimulate SOs in the OFC, which then propagate to other cortical areas, possibly generating additional SOs in other regions. Models 3 and 4 would both suggest some kind of early auditory evoked response within the OFC, but would differ in the direction of functional connectivity between AC and OFC.

In the present work, we evaluate evidence in favour of each of these models using magnetoencephalography (MEG), a temporally and spatially-resolved neuroimaging technique which allows us to explore the relative timing and amplitude of brain responses across brain regions (Baillet, 2017). We recorded MEG and EEG data simultaneously in an overnight design, in five healthy young adults, while short, quiet sounds were presented. We measured brain responses to sound across sleep stages and as a function of their phase relationship with endogenous SOs. We also explored the relationship of the MEG results to the signal observed in single-channel EEG, as it is most frequently used both to detect SOs and assess the impact of CLAS-SO on evoked oscillations, in extent research. Clarifying how sound stimulates the brain has important implications for making causal manipulation tools like CLAS more effective in fundamental research and in potential clinical applications.

Methods

Participants. Six neurologically healthy young adults without sleep nor neurological conditions were recruited from the local community. One dataset was unusable due to a technical problem with the EEG system that precluded scoring. The mean age of the five remaining participants was 21.2 (SD: 1.33; range 19-23), and 3 were female. All subjects reported being in good health with normal hearing, were non-smokers, were not taking medication, had not changed time zones or conducted shift work in the 6 weeks preceding the experiment, and had a normal 6-10 hour sleeping pattern in the three days prior to the experiment (confirmed by sleep log). The night prior to the experiment, participants were asked to stay up one hour later than their habitual bedtime to increase sleep pressure. The day of the experiment they were asked to refrain from consuming caffeine, alcohol, nicotine, and cannabis. Subjects gave written informed consent, and were compensated for their time. The experimental protocol was approved by Concordia University's Human Research Ethics Committee, and the Research Ethics Board at McGill University.

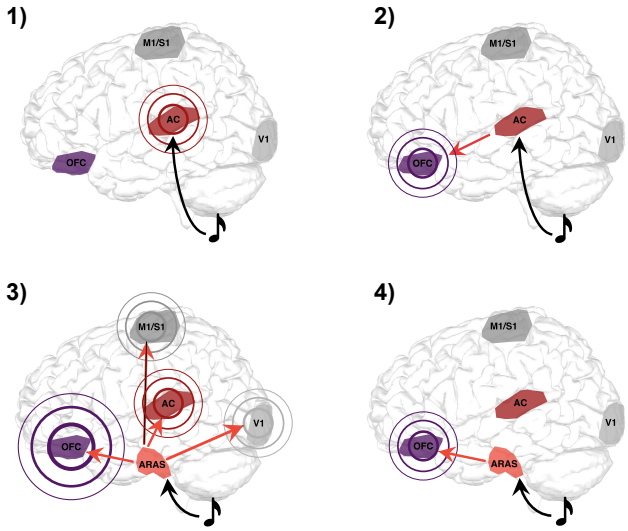

Fig. 1. Four models of information flow leading to generation of evoked slow-oscillations. 1) SO is evoked by arrival of auditory information in the AC via auditory pathways, from which it propagates. 2) Auditory information arrives in the AC, spreads in cortico-cortical networks to the OFC, which is sensitive to stimulation in sleep and generates SOs, from whence they propagate. 3) The arousal networks in brainstem and thalamaus are stimulated, and generate widespread and simultaneous SOs, most strongly in OFC due to its sensitivity. 4) Arousal system is activated as in 3, but SOs are generated first in OFC, from which they propagate to other brain areas.

Study design. On the experimental evening, participants first completed a health questionnaire to confirm eligibility; the Munich Chronotype Questionnaire (MCTQ) to document their habitual diurnal rhythms (Roenneberg et al., 2003); and the Pittsburgh Sleep Quality Index (PSQI) (Buysse et al., 1989), which contains 19 self-rated questions which are scored from 0-3 points, where '0' indicates no difficulty, and '3' indicates severe difficulty. The PSQI seven component scores are added to yield a global score between 0 and 21 points. Scores of 5 or more indicates poor sleep quality; the higher the score, the worse the quality. Participants also completed a subjective fatigue scale concerning their current state, which consisted of 7 questions rated on a 5 point Likert-scale. Items on the scale asked about subjects' levels of tiredness, activity, motivation, interest, concentration, relaxation and general feeling; all ratings were moderate.

Participants were prepared for EEG with electrodes positioned at Cz, C3, and C4; 10-20 system (Homan et al., 1987). To avoid discomfort due to contact with the MEG helmet, occipital electrodes were not used. Participants settled into the MEG scanner in a supine position. A five-minute resting state data acquisition with eyes open was collected, as a contribution to an open-access database (which also houses the current dataset (Niso et al., 2016)). Lights were dimmed to full darkness, and subjects were asked to close their eyes and relax. Sound stimulation was started immediately, with the subject in the awake state, to allow them to get used to the sound and so that the brain response to the wake state could be measured. Standard T1-weighted magnetic resonance anatomical images (1 mm^3 isotropic voxels) were acquired in a separate session to enable distributed source localization of MEG signals.

Auditory stimulation. We used a 120 ms synthetic speech syllable (/da/, 10 ms consonant burst, a 30 ms formant transition, and an 80 ms steady-state vowel with a fundamental frequency of 98 Hz), to facilitate comparison of the evoked responses in simultaneously acquired EEG and MEG with previous work (Coffey et al., 2016, 2017, 2021). The stimulus was presented binaurally through Etymotic ER-3A insert earphones with foam tips (Etymotic Research), at 55 dB SPL, which we determined through pilot testing was clearly audible but did not awaken sleeping participants. The stimulus onset interval range was 2800 to 3000 ms (mean $\sim$2900 s), where jitter was selected randomly from a uniform distribution.

EEG and MEG data collection. Two hundred and seventy MEG channels (axial gradiometers), five EEG channels (C3, C4, Cz, M1 and M2), EOG, ECG, and one audio channel were simultaneously acquired using a CTF MEG System and its in-built EEG system (Omega 275, CTF Systems Inc.). All data were sampled at 2400 Hz, and were recorded in 30-minute 'runs'. Prior to each run, the head was localized, and head position was stored for use in MEG source localization. Data pre-processing

was performed with Brainstorm (Tadel et al., 2011), and using custom scripts (The Mathworks Inc., MA, USA), according to recommended practices (Gross et al., 2013).

Sleep scoring. Sleep scoring of the data, in which 30 s windows of data are visually inspected and categorized into wake, non-REM sleep stages 1-3, and REM sleep, was accomplished according to AASM practices (Iber, 2007) based on band-pass filtered EEG (0.1-20 Hz, channels 'C3', 'C4', and 'Cz' referenced to left mastoid), EOG (0.1-5 Hz), and EMG (10-58 Hz) channels, which were then down-sampled for ease of handling to 150 Hz. Each epoch was scored by one researcher and confirmed or challenged by a second observer. Discrepancies were resolved via discussion.

Statistical approach. We elected to study a small number of subjects in an overnight design rather than a larger number of subjects for shorter sleep periods (as is used most nap studies and studies investigating behavioural correlates) so as to be able to capture brain responses across all sleep stages, and to have a very high number of stimulations per subject that hit sleep features of interest (e.g. SO troughs and peaks), or missed them (e.g., stimulations that occurred in the absence of SOs, spindles, and their refractory periods). This design also facilitated an in-depth exploration of phase relationships between EEG and specific brain regions. It is increasingly being recognized that statistical power is dependent upon the amount of data available per subject, particularly in cases in which the within-participant variance is larger than the between-participants variance (Baker et al., 2021). The approach of collecting a large amount of data in a small number of subjects is best suited to research questions that address low-level mechanisms that are likely to be highly similar across participants. It has a long history in non-human primate research, in which research resources and ethical considerations limit sample sizes (please see Baker et al. (2021), Brysbaert and Stevens (2018), Smith and Little (2018) for a discussion and demonstration of the trade-offs between number of subjects and number of observations).

Analysis for basic confirmations of well-established results (e.g., the presence of an evoked N550-P900 complex in NREM sleep stages 2 and 3) were conducted using non-parametric Wilcoxon signed-rank tests on subject means. With our small number of subjects, these results are valid, but are only significant if all five subjects show the same pattern of results. They serve only to confirm that well-replicated phenomena (like the existence of a N550-P900 complex in sleep) are clearly and consistently observed across subjects in this study, as a starting point for addressing the study's specific objectives. Each subject's mean values across conditions were normalized by dividing their maximum value, for visualization purposes.

For the main research questions, we applied linear mixed effects (LME) models (Pinheiro and Bates, 2006), which model the relationship between dependent data and independent data when there is a correlation between observations (e.g., multiple measurements taken from each subject; subject is modelled as a random factor). This class of models takes advantage of the high number of observations per subject (i.e., between 5,000 and 116,000 depending on the research question). LME analyses were conducted in R using the lme4 and emmeans packages (Bates et al., 2015, Lenth, 2022). Alpha values of .05 were used throughout, and FDR corrections for multiple comparisons were applied over the dimensions of interest (e.g., frequency bins) when necessary, using the Benjamini-Hochberg procedure (Thissen et al., 2002). For each linear mixed effects models used in analysis, we visually inspected the histograms and quantile-quantile (Q-Q) plots of the residuals for deviations from normality and homoskedasticity. In models in which clear deviations were present, we excluded outliers by removing values based on thresholds that were defined as 1.5 times the interquartile range (i.e., below Q1 and above Q3; this methods removes data which lie beyond 2.7 σ from the mean), and re-ran the models. The use of outlier removal is indicated for each analysis.

EEG auditory evoked responses across sleep stages. For EEG analysis, we used a 'Cz' to left mastoid channel. We first filtered the raw data between 0.1 and 200 Hz (87010-order linear phase FIR (finite impulse response) filter with a Kaiser window and 60 dB stop-band attenuation; the order is estimated using the MATLAB 'kaiserord' function, and filter delay is compensated by shifting the sequence to effectively achieve zero phase and zero delay, as per Brainstorm default settings (Tadel et al., 2011)). Data were then down-sampled to 500 Hz, epochs from 1 second pre-stimulus onset to 3 seconds post-stimulus onset were extracted, and the mean during the pre-stimulus baseline period was subtracted from each epoch. Epochs were separated according to the sleep stage during which they occurred, and grouped across an individual's runs. Subject averages were computed for each sleep stage, a 40 Hz low-pass filter was applied to the average so as to maximize comparability with

previous work looking at auditory evoked responses, and mean values from -0.5 s to 0 s were subtracted for better visual alignment across sleep stage time series. Grand average means and standard error were computed for each time series, for visualization purposes.

To quantify the amplitude of the P200 ERP component, we computed average amplitude for each stage between 165 and 205 ms (based on a previously-observed P200 peak in both EEG and MEG to the same stimulus at ∼185 ms (see Coffey et al. (2017)). The latency of the N350 component appeared to increase in deeper NREM sleep stages (see Figure 2). For Wake, N1, and REM, we used a window of 240 to 280 ms; for N2, the window was defined as 265 to 305 ms, and for N3, 290 to 330 ms after sound presentation. To compute the amplitude of the slowest evoked responses, we first averaged a time window 500 to 600 ms to capture the N550 component, and 800 to 1000 ms for the P900 component. We then subtracted the N550 mean value from the P900 value to get an amplitude measure of the N550-P900 complex. Note that we favour this terminology when referring to activity occurring within this time window to avoid assumptions about whether or not K-complexes are evoked on individual trials. However, 'P900-N550' is used in figures to indicate the direction of subtraction in the case the amplitude difference between the two components is measured (i.e., P900 amplitude minus N550 amplitude, which results in a positive peak-to-trough value in case of a successful evoked response).

Later components have broader peaks and are generally less temporally-aligned across subjects, motivating the use of longer windows. We used simple non-parametric Wilcoxon signed-rank tests (one-tailed) to test whether the amplitudes of P200, N550, and N550-P900 complexes differed in N2 and N3 sleep as compared with responses within each time window during wakefulness. We calculated effect sizes for between-condition comparisons used the probability of superiority (PSdep), which is calculated as the number of positive difference scores divided by the total number of paired scores (Grissom and Kim, 2012).

Because CLAS is thought to affect memory through the generation of not only slow oscillations, but also sleep spindles nested within them (Ngo et al., 2013), we also investigated changes in spindle band power following sound stimulation, across sleep stages. For each epoch, we computed time-frequency power over a 1-30 Hz frequency band (central frequency: 15 Hz, full-width half-maximum: 0.2 s), using spectral flattening (i.e., power values are multiplied by frequency), in Brainstorm (Tadel et al., 2011). All epochs were averaged by sleep stage within subjects, and a subject grand average difference for N3 minus Wake was computed to define a time and frequency window of interest for further analysis, by visual inspection, which was 0.6-1.2 s after sound onset in a 11-14 Hz frequency band. We then computed the difference between this window and an equivalent window preceding sound offset (-0.6-0 s after sound onset, 11-14 Hz), for each subject and sleep stage. As above, we used a non-parametric Wilcoxon signed-rank test (one-tailed) to confirm that spindle power amplitude increased across subjects following sound presentation as compared with baseline, specifically in N3 when the effect should be most prominent, and in N2 as a basis for merging of N2 and N3 epochs. These EEG-based analyses serve to select parameters (e.g., time and frequency windows) for further analysis in MEG source space.

In past work, epochs have sometimes been divided into those which produce a strong response (K-complex), and those which do not (e.g., Bastien and Campbell (1992), Dang-Vu et al. (2011)). To explore whether evoked responses are unimodally or bimodally distributed, as would be the case in an all-or-nothing response, we selected stimulations which fell into N2 and N3 sleep stages, yet coincided neither with a slow oscillation nor sleep spindle (as measured in the Cz-to-mastoid EEG channel). We extracted average amplitudes for each epoch during the N550 and P900 windows (as in the analysis above), and computed their difference as a measure of the strength of the N550-P900 complex. We then plotted the distribution of trough-to-peak amplitudes for each subject. Epochs were then sorted into those containing the top 25% and bottom 25% amplitude values. To investigate the relationship between elicited N550-P900 complex and spindle generation, time-frequency plots were computed and averaged for each condition and each subject. Each subject's mean values across conditions were normalized by dividing their maximum value, for visualization purposes.

SO detection and phase-binning. We used a Cz-to-mastoid channel to detect slow oscillations using an offline detection algorithm developed by Carrier et al. (2011). In brief, EEG was filtered between 0.16 and 4 Hz and four criteria were evaluated to detect the emergence of a slow oscillation: a peak-to-peak amplitude greater than 75 μV, a negative peak amplitude higher than 40 μV, a duration of the negative peak between 125 and 1500 ms, and a positive peak lasting less than 100 ms (Rosinvil

et al., 2021). Detected slow oscillations were then divided into bins representing cortical states.

To explore the impact of up-states and down-states of slow oscillations and question the mechanism of CLAS, 150 ms time windows centred on the detected peak and trough of each oscillation were defined and stimulation occurring approximately simultaneously (defined as occurring within a 150 ms window centred on the detected peak or trough) were sorted accordingly 'Up-state' and 'Down-state' categories. Stimulation occurring outside of a detected slow oscillation (or sleep spindles and their associated refractory periods) was sorted into an additional bin referred to as 'Clear'. Based on the definition by Antony et al. (2018), the spindle refractory period was defined as a fixed time window lasting 2.5 seconds after the offset of the detected sleep spindle. To maximize the number of stimulations per bin, we combined N2 and N3 NREM sleep stages. On average, the number of stimulations during detected slow oscillations per subject across all phases was 411.8 (SD = 180.7, range = 196-608), and the number of stimulations during the 'Clear' condition was 2055.5 (SD = 535.6, range = 1474-2764).

Spindle detection. Sleep spindles were detected as input to sort stimulations into the Clear condition, such that they coincided neither with a slow oscillation nor with a spindle. Sleep spindles were detected on the Cz (referenced to mastoid) channel, because it is centrally located, near where spindles peak (Cox et al., 2017). Spindles were detected offline using an algorithm which emulates human scoring (Lacourse et al., 2019). In brief, the algorithm filters the EEG signal in the sigma band, 11-16 Hz (as per Lacourse et al. (2019)), and applies four criteria: absolute sigma power (default = 1.25), relative sigma power (default = 1.6), and both correlation (default = 0.6) and covariance (default = 1.3) of the sigma band-passed signal to the original EEG signal. After consultation with the authors, we adjusted the parameters slightly to work better with our EEG data (absolute sigma power = 0.8; relative sigma power = 1.0; covariance = 1.0; correlation = 0.4), and a trained expert confirmed successful detection visually for each subject. As in the analysis of slow oscillations, N2 and N3 sleep stages were merged.

MEG data processing. Cardiac artifacts were removed from MEG data using Brainstorm's in-built cardiac detection and source signal projection algorithms (Tesche et al., 1995). Projectors were removed when they captured at least 12% of the signal and the topography of the components matched those of ocular or cardiac origin upon visual inspection. Eye blinks were not detected nor removed, as participants generally had their eyes closed during the recording. Data were filtered between 0.1 and 200 Hz, and down-sampled to 500 Hz. For ERP and ERF analyses, data were further low-pass filtered below 40 Hz, which is common practice to measure the amplitude of evoked auditory response components (e.g., P200). Auditory event markers were used to define epochs that started 1 s before sound onset and ended 3 s after sound onset as in the EEG analysis. Similar to previous work (Coffey et al., 2021), we used a distributed source-modelling approach. This process estimates activity originating throughout the brain, constrained by spatial priors derived from each subject's T1-weighted anatomic MRI scan (Baillet et al., 2001, Gross et al., 2013). We imported anatomical data into Brainstorm, and cortical and subcortical (thalamus, hippocampus, and amygdala) structures were combined with the cortex surface ($\sim$15,000 vertices). An overlapping-sphere head model was computed for each run; this forward model explains how an electric current flowing in the brain would be recorded at the level of the sensors (Tadel et al., 2011). A noise covariance matrix was computed from 2 min empty-room recordings taken before each session. We computed the minimum-norm estimate (MNE) source distribution model using source orientations constrained to brain structure surfaces, for each run (Hämäläinen, 2009). Source models for each run were averaged within-subject.

MEG topographies. To explore the topography of the evoked slow oscillations (as indexed by N550-900 complex amplitude), we prepared subject averages in source space for stimulations occurring in Wake, N2, and N3 sleep stages, and extracted time series using the Destrieux brain atlas (Destrieux et al., 2010). As our source models included thalamus, hippocampus, and amygdala in addition to the cortex, we created ROIs for these areas. Because the first two structures are large and averaging source-spaced signals over large, elongated or round regions can degrade the signal, we divided them each into three equally-sized ROIs, and visually confirmed that each subject's divisions were similarly positioned and numbered, thus roughly corresponding across subjects and allowing for meaningful group averages. To maximize the number of trials and thus signal clarity for the sleep analyses, we calculated a weighted average across N2 and N3 sleep stages, proportional to the amount of N2 and N3 sleep collected for each participant (see Table 1). We then created weighted grand averages for each of the

Destrieux regions of interest for Wake and combined N2 and N3 sleep ('N2 & N3'), taking into consideration the proportion of data recorded for individual participants. Each ROI time series was baseline-corrected (-0.5 to 0 s relative to stimulus onset). The amplitude of the N550-P900 complex was computed as described in the EEG analysis (i.e., an average over 500-600 ms was subtracted from an average over 800-1000 ms), and the absolute value was taken. A difference was then computed between the Wake and N2 & N3 conditions. ROIs having outlying values +/- 3SD of the mean across all ROIs was set to +/-3SD, and the values were mapped to colour scales such that red indicates greater activity change relative to pre-stimulation baseline, in sleep). To explore the spatial trajectory of brain activity over time in NREM sleep, we conducted a similar analysis, except that brain activity was computed over six consecutive 500 ms windows starting at -0.5 s relative to stimulation, and the absolute value over each window was displayed on a black-to-red colour scale where red indicates more activity change relative to the pre-stimulus baseline period.

To explore the topography of evoked responses in the spindle range, we computed spindle band power as in the EEG window in Wake and NREM (N2&N3) for each region of interest, and mapped the power difference to a blue-red scale where red indicates more spindle activity in sleep. These average activity topographies were used to present spatial information concerning evoked responses qualitatively, and as input to confirm and select regions of interest for further investigation of evoked responses in source space.

For a visual comparison of the topography of the evoked slow responses and spindle band activity, we used the FOOOF algorithm (https://fooof-tools.github.io/fooof/) as implemented in Brainstorm (frequency range of analysis: 1-40 Hz; otherwise using default parameters: peak width limits: 0.5-12 Hz, maximum number of peaks: 3, min peak height = 3 dB, proximity threshold: 2 standard deviations) to separate oscillatory from 1/f (frequency) brain activity (Donoghue et al., 2020), and averaged peak values for slow oscillations (0.5-1.5 Hz) and spindles (11-17 Hz) separately. We used the wider spindle frequency range here for best comparison with prior literature, although it is slightly different than the 11-14 Hz range selected based on the evoked spindle power in our own dataset. Note that due to the study design, brain activity captured in this analyses includes a combination of evoked and endogenous activity, meaning that we limit our analysis to a qualitative observation of similarities; a specialized study design that clearly separates evoked from endogenous oscillations would be needed to quantitatively investigated questions of similarity more thoroughly. Note that endogenous slow oscillations and stimulus-evoked K-complexes share many similarities and there is currently no normative data for discriminating evoked responses from other slow waves (Halász, 2016).

MEG time series analysis. Based on the models that we propose to evaluate (Figure 1) as well as the topographical analyses showed in Figure 4, five bilateral cortical regions of interest (ROIs) based on the Destrieux atlas (Destrieux et al., 2010) were defined in subject space for each participant. The selected ROIs are based on: 'pre-central gyrus', 'post central gyrus', 'occipital lobe', and 'sub-callosal gyrus', and the 'transverse temporal' and 'planum temporale' gyri, which were merged to capture the auditory cortex. Each ROI was defined in each hemisphere. The size of each ROI was manipulated by progressively increasing or decreasing ROI area, so as to be similar across ROIs and hemispheres (across all ROIs, all subjects, mean area: 10.3 cm^2, SD: 0.2 cm^2, range: 9.99 to 10.88 cm^2). We preferred to use ROIs of similar size, as we extract the mean activity from each ROI.

For MEG analysis investigating the contribution of specific ROIs, we sorted epochs (i.e., -1 to +3 s relative to sound onset) by sleep stage, and produced evoked response plots, as in the EEG analysis (see Supplementary Figure 1). To evaluate the presence or absence of specific peaks in the evoked response, we then measured the mean amplitude over a window centered on P200 in EEG (165 and 205 ms post stimulation) as well as the difference in amplitude within a time window capturing the N550-P900 slope as observed in EEG ERPs (i.e., the average amplitude over 500ms to 600 ms subtracted from the average amplitude from 800ms to 1000ms) for each run and for each ROI. Extracted values for each epoch were then used in LME statistical models to assess the impact of sleep stage on responses elicited by sound across sleep stages.

Directed phase-transfer entropy. Functional connectivity between the AC and OFC was estimated using directed phase-transfer entropy (dPTE) (Lobier et al., 2014). In brief, the time series is described by its instantaneous phase, in a similar fashion to Wiener-Granger causality (Hillebrand et al., 2016). Signals were first band-pass filtered in frequency bands (i.e., 0.5-

1.5, 2-4, 5-7, 8-10, 11-17, 18-29, and 30-58 Hz). These frequency band divisions are those normally labelled as 'delta', 'theta', 'alpha', 'beta' and 'low gamma', with the additional separation of 0.5-1.5 Hz and 11-17 Hz as slow oscillation and spindle or 'sigma' bands, due to their relevance to the research questions. Directed phase-transfer entropy was computed for each pair of ROIs within each frequency band, and normalized between -0.5 and 0.5. The sign of the result indicates the dominant direction of functional connectivity. Directed phase-transfer entropy results for each trial were then entered in LME statistical models.

Up-state and down-state detection in EEG and MEG. We explored the role of tissue state in specific regions and its relationship to EEG by detecting up and down-states in extracted time series from each ROI over each $\sim$30 min recording. We used the same detection algorithm for the MEG data (extracted from regions of interest in source space) as had been used for EEG (Cz) signals, to maximize comparability. We first isolated periods of sleep that had been manually scored as N2 or N3, and filtered the data in the slow wave frequency band (0.1 to 2 Hz). Troughs and peaks were automatically detected (using the 'findpeaks' function implemented in MATLAB), and the amplitude difference between peak and trough amplitude was computed for each detected peak. Trials were sorted by amplitude differences, and epochs containing the top 25% of peak-trough amplitude for each subject were selected as our Up-state condition for further analyses. Similar processing pipeline was used to select troughs (Down-states) by detecting peaks after inverting the signal (i.e., multiplication by -1).

Epochs were defined around the detected peak (Up-state) in the EEG signal (-2 to +2 s) to examine the correlation between the EEG signal and MEG signal extracted from ROIs. Correlation of the signal from the EEG sensor Cz and each extracted signal was then computed and the correlational relationship between signals was investigated using LMEs. The instantaneous phase of the signal in EEG as well as in each ROI was extracted using the Hilbert transform of the signal.

Finally, to investigate the role of cortical tissue excitation state on EEG brain evoked responses, incoming sounds were sorted according to whether they coincided with a local up-state or down-state in each ROI (as defined by a 150 ms window centred on the detected peak or trough), and as before, 4 s epochs (-1 s pre-stimulation onset to 3 s post-stimulation onset) were defined. The elicited N550-P900 complex amplitude was measured as previously described and the sigma power post-stimulation was calculated using the root mean square (RMS) value of the signal filtered between 11 and 14 Hz, 0.6 to 1.2 s after stimulation from which a pre-stimulus value (-0.6 to 0 s) was subtracted to emphasize sound-evoked spindle band power, as in previous analyses.

Results

Sleep. All subjects were able to sleep in the physically-restricted and unfamiliar scanner environment. Sound stimulation was started before sleep onset and all subjects were able to fall asleep, but as sleep pressure wore off, participants sometimes reported that when they awakened, the stimulation distracted them from falling asleep again. Participants could ask for the stimulation to be turned off until they were once again asleep. Unstimulated periods were not included in the analyses and 30 s epochs containing movement were discarded. On average, participants had 246.6 mins of movement-free, stimulated recordings (SD = 26.6 mins). Every subject, except one ('Sub2'), had >10 mins of N3 and REM sleep. See Table 1 for details. In analyses which combined N2 and N3, weighted averages within-subject were used to account for the differences in sleep stage duration.

Effect of sleep stage on brain responses evoked by auditory stimulation.

Auditory evoked responses in EEG. The evoked responses for each observed sleep stage in EEG, averaged across subjects, are presented in Figure 2a. Qualitatively, the early evoked responses that are associated with auditory processing in wake states (i.e., P100, N100, P200) do not appear to be strongly influenced by sleep stage, whereas the later components (i.e, N350, N550, P900) that appear only in sleep are stronger in deeper NREM stages.

We used simple non-parametric Wilcoxon signed-rank tests (one-tailed) to evaluate whether evoked response amplitudes differed between wakefulness and deeper NREM sleep stages (N2 & N3), which are the brain states in which CLAS of SOs is normally used. P200, as a representative measure of the classical auditory evoked response, was significantly greater in N2 sleep as compared to wake ($Z = 15$, $p = .03$, PSdep = 1.0), but the Wake vs. N3 difference was not significant ($Z = 3$, $p = 0.31$, PSdep = 0.8). The N350 component, instead, was significantly larger in NREM sleep stages 2 and 3 ($Z = 15$, $p = .03$,

Table 1. Sleep staging results from usable recordings during which sound stimulation was present, for each subject. Sleep was staged into 30 s epochs, and reported in minutes per stage. The number of auditory stimulations occurring during each stage is reported in parentheses.

Subjects	Wake min (#)	N1 min (#)	N2 min (#)	N3 min (#)	REM min (#)
Sub1	30.5 (610)	12 (235)	99 (1979)	107.5 (2157)	21 (420)
Sub2	32 (487)	152 (2439)	83 (1479)	7 (137)	0 (0)
Sub3	125 (2493)	31 (607)	66.5 (1321)	89 (1766)	21.5 (431)
Sub4	15 (145)	6.5 (46)	55.5 (579)	186.5 (3368)	23.5 (470)
Sub5	49.5 (913)	55 (994)	121 (2236)	82 (1601)	13.5 (272)
Average	50.4 (929.6)	51.3 (864.2)	85 (1518.8)	94.4 (1805.8)	15.9 (318.6)
Std	43.43 (916.3)	59.4 (952.4)	26.05 (642.3)	64.18 (1161.1)	9.7 (193.3)

PSdep = 1.0 for both). The N550-P900 complex (i.e., P900 - N550 amplitude) was significantly greater in N3 sleep than Wake (Z = 15, p = .03, PSdep = 1.0), but did not reach significance in N2 sleep (Z = 14, p = .06, PSdep = 0.8). These results are used to confirm that the slow evoked responses that emerge in deeper sleep (N2 and N3) and have been previously reported (see Bastien et al. (2002), Colrain and Campbell (2007)) are present in our sample, as a starting point for spatially-resolved MEG analyses. To increase the number of trials for subsequent analyses, we combine N2 and N3 sleep stages, as N350 and N550-P900 components are observed in both stages (Colrain and Campbell, 2007) (although noting that the N2 effects are smaller than in deeper, N3 sleep). Importantly for the purposes of using LME models, the number of observations included in the statistical analyses for the main questions concerning the effects of sound stimulation in N2 and N3 sleep are over 16,000 per region of interest (see Table 1).

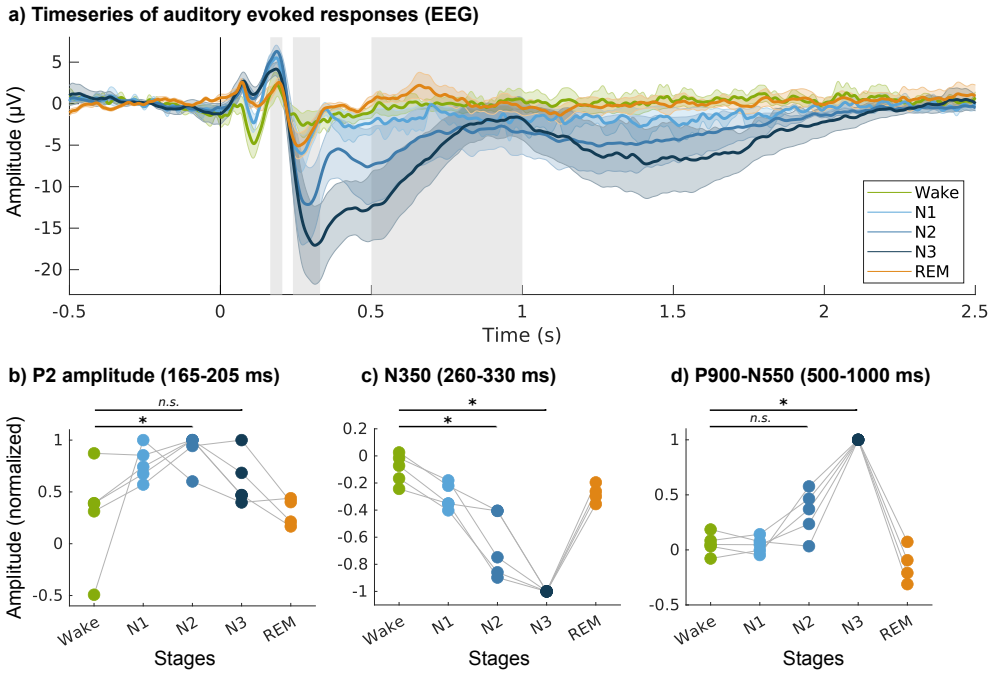

Fig. 2. Evoked responses over sleep stages, in EEG (Cz). a) Time series of the auditory evoked responses showing the appearance and evolution of late evoked components (N350, N550, P900) in deeper NREM sleep stages. Coloured lines show means across participants; shaded areas indicate standard error. Grey rectangles indicate time ranges of interest that are used for further analysis. Asterisks denote significant differences between Wake and deeper sleep conditions (Wilcoxon signed-rank test on the means; p < .05). b) Amplitudes of the P200 component show little change across sleep stages. Conversely, amplitudes c) at N350 and d) peak-to-trough differences between P900 and N550 are stronger in deeper NREM sleep stages than in Wake.

Slow oscillations evoked by sound in sleep in MEG source space. The topography of evoked activity differences between Wake and N2 & N3 is displayed in Figure 3. Widespread activity differences are observed in ventral and orbital frontal

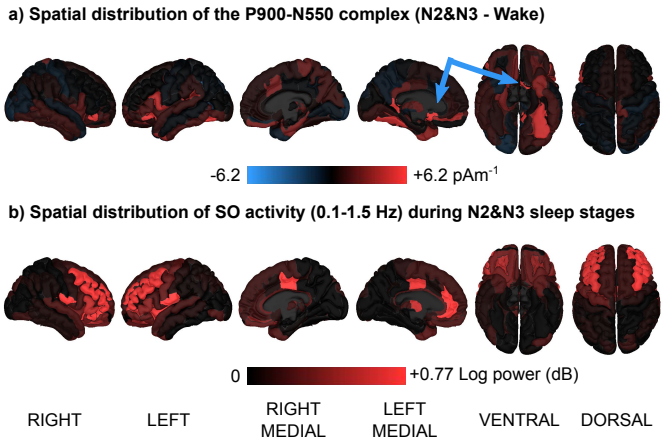

Fig. 3. Topographies of a) evoked activity differences between wake and NREM sleep (stages N2 and N3 combined). Red indicates more activity change relative to pre-stimulus baseline during the auditory-evoked N550-P900 complex in sleep as compared to wake. The evoked N550-P900 complex is specific to sleep and shows widespread activity change in ventral and orbital frontal areas (see also Figure 2b,d for topographies of evoked activity in NREM sleep over time). b) Topography of slow frequency oscillatory activity during N2 & N3 sleep stages (as indexed using FOOOF), for reference.

regions, and inferior frontal gyrus (e.g., Destrieux regions 'G_subcallosal L', 'Lat_Fis-ant-Vertical L', 'G_cingul-Post-ventral L', 'G_front_inf-Orbital R', 'S_circular_insula_ant L'). On the basis of these observations, we selected Destrieux atlas regions ('G_subcallosal' left and right) as representative of ventral regions exemplifying the SO evoked response (see Methods for details, and Figure 6b for a visualization of the resulting ROI). For visual comparison only, we plotted topographies of slow frequency oscillatory activity during N2 & N3 stages (FOOOF). In general, we observed some overlap between the evoked N550-P900 complex topography (Figure 3a) and the slow oscillation activity (Figure 3b); however, there was more SO activity in dorsolateral frontal regions. As noted in methods, the specific study design does not allow us to clearly separate (and therefore quantitatively compare) evoked vs. endogenous SO topographies. We also take advantage of magnetoencephalography's temporal resolution to visualize the time course of the evoked responses, see Figure 4. In the earlier time window (0 to 0.5 s), the auditory cortex is bilaterally active. In later periods (e.g., 1.5 to 2.0 s), the orbitofrontal regions show greater change with respect to pre-stimulus baseline. The auditory regions also show activity changes in later periods. Note that the P900 component is not prominent in this representation, which displays difference from baseline, because as shown in the time series average (Figure 4 (bottom)), amplitude peaks close to the pre-stimulus level (at 0.9 s) before once again decreasing (at 1.5 s).

To better characterize the sound-evoked N550-P900 complex, we investigated whether it represents an 'all-or-none' response, as suggested by some previous work in which epochs have been separated according to the presence or absence of an elicited N550-P900 complex (e.g., Bastien and Campbell (1992), Dang-Vu et al. (2011), Laurino et al. (2014)). In closed-loop auditory stimulation applications, up-states are preferentially stimulated as they produce the greatest enhancement in slow oscillations and evoked spindle power (Ngo et al., 2013). In the current analysis, however, we focused on periods of time in which sound presentation did *not* coincide with slow oscillations or sleep spindles (in EEG), to observe the evolution of the evoked response in the absence of endogenous sleep-related events (later sections explore the effect of cortical tissue excitability on the EEG evoked response).

We first identified trials that occurred within spindle and SO-free stage N2 & N3 sleep (as identified by automatic detection algorithms). The mean number of trials included per participant was 2284.2 (SD = 650; individual totals: Sub1 = 2762, Sub2 = 1325, Sub3 = 1910, Sub4 = 2850, Sub5 = 2574). In general, each subject's N550-P900 complex amplitude distribution was centred around zero (means (SD) by subject: Sub1: 4.76 μV (43.2), Sub2 = -.04 μV (22.1), Sub3 = 4.54 μV (42.5), Sub4 = 14.89 μV (54.3), Sub5 = 4.26 μV (37.7)). Interestingly, we do not observe a bimodal distribution that might suggest that sound produces a clear evoked slow oscillation in a binary fashion (see Supplementary Figure 2); however, to examine the relationship between evoked N550-P900 amplitude and spindle-band activity, we nonetheless separated trials into those producing relatively higher amplitude N550-P900 complexes (i.e., top 25%) and those which had lower values during the same time window (i.e., bottom 25%).

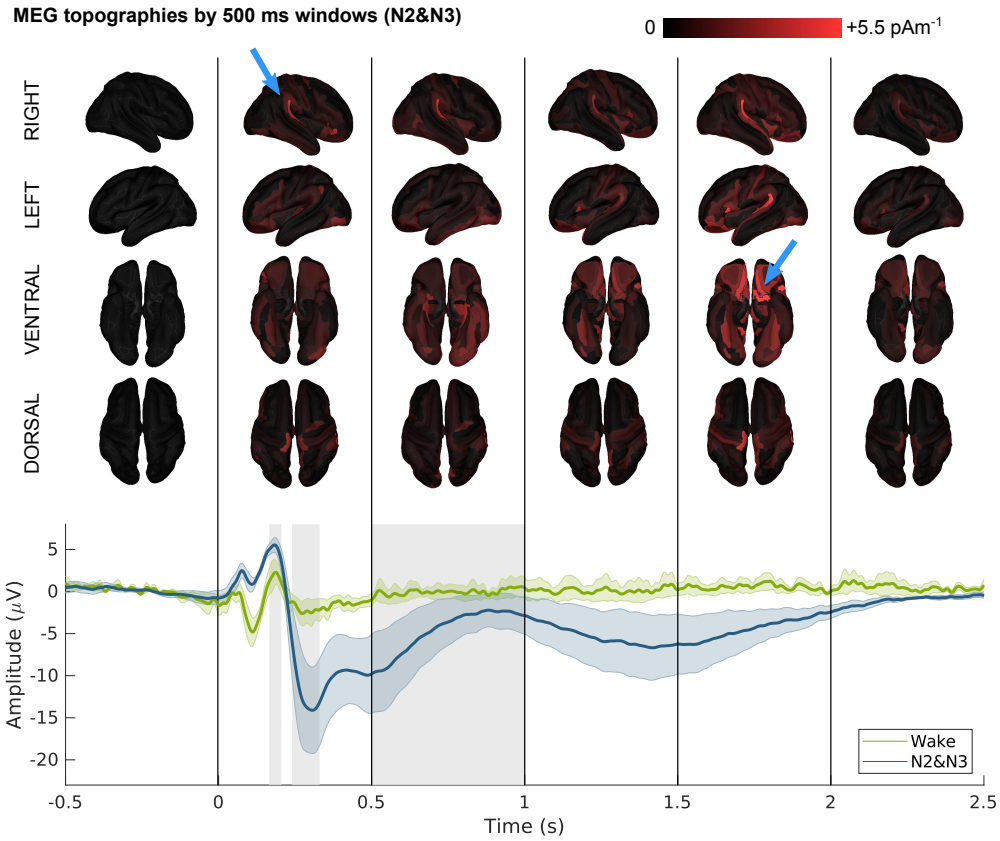

Fig. 4. Topographies of evoked activity in NREM sleep over time (stages N2 & N3 are combined). Brighter red indicates relatively more activity change relative to pre-stimulus baseline. The EEG time series of evoked responses for Wake and N2&N3 is shown (bottom) for reference.

Sleep spindles evoked by sound in sleep. To evaluate differences in how sound evokes sleep spindles across stages of consciousness, we calculated mean time-frequency plots for Wake and N2 & N3 across all subjects and epochs, and computed their difference, to identify a time and frequency window for further analysis (see Figure 5a). Evoked responses were maximally different between Wake and N2 & N3 starting about 0.6 s and ending about 1.2 s after sound onset, and within a 11-14 Hz frequency band, by visual inspection. Although the axis is dominated by a particularly strong responder (see Figure 5a (right)), all subjects showed greater spindle power in N2 & N3 than Wake using simple non-parametric Wilcoxon signed-rank tests (one-tailed) across subject means (Z = 15, p = .031, PSdep = 1.0). Interestingly, the strong responder who showed the greatest evoked spindle-band power in N2 & N3 sleep was the same as the one who had exaggerated responses within N350 and N550-P900 complex (Figure 2d), and seems to have slept most deeply, with the longest duration of N2 & N3(Table 1).

To more robustly evaluate differences in evoked spindle power as a function of the N550-P900 complex's amplitude, we conducted LME analyses at the single trial level, using subjects as a random effect. We removed outliers from each Condition (Top 25%, Bottom 25%) by excluding values based on thresholds defined as 1.5 times the interquartile range (i.e., below Q1 and above Q3). The mean percentage of retained epochs across subjects was 95.8% (SD = 4.0). We compared a model with N550-P900 complex's amplitude Condition (either Top 25% or Bottom 25%) as a fixed effect to a null intercept-only model and found that the addition of the Condition significantly increased model fit ($\chi^2(1) = 67.04$, $p < .0001$). The intercept estimates the mean spindle power increase post-stimulation generating low amplitude N550-P900 complexes (Bottom 25% condition). There was a significant main effect of Condition, indicating statistically stronger spindle power in the Top 25% of epochs than in the Bottom 25% of epochs (β = 3.83e-01, SE = 4.66e-02, t(5454) = 8.21, $p < .0001$).

The topography of evoked spindle activity differences between Top vs. Bottom 25% of evoked N550-P900 complexes is displayed in Figure 5c. Increased activity was observed mainly in medial regions (e.g., Destrieux regions 'G_cingul-Post-dorsal', 'G_and_S_cingul-Mid-Ant', 'G_cingul-Post-dorsal , 'S_subparietal'), and also in lateral occipital regions (e.g., 'G_and_S_occipital_inf'). An increase in thalamic activity is also observed. For visual comparison only, we plotted topogra-

phies of spindle-band (11-17 Hz) oscillatory activity during N2 & N3 stages (using FOOOF). In general, we observed considerable overlap between the evoked spindle topography as described above (Figure 5c) and activity measured in the spindle band across N2 and N3 sleep stages using the FOOOF algorithm (Figure 5d), with the strongest activity observed in medial regions. As noted in Methods, the study design does not allow us to cleanly separate and therefore quantitatively compare evoked vs. endogenous spindle topographies.

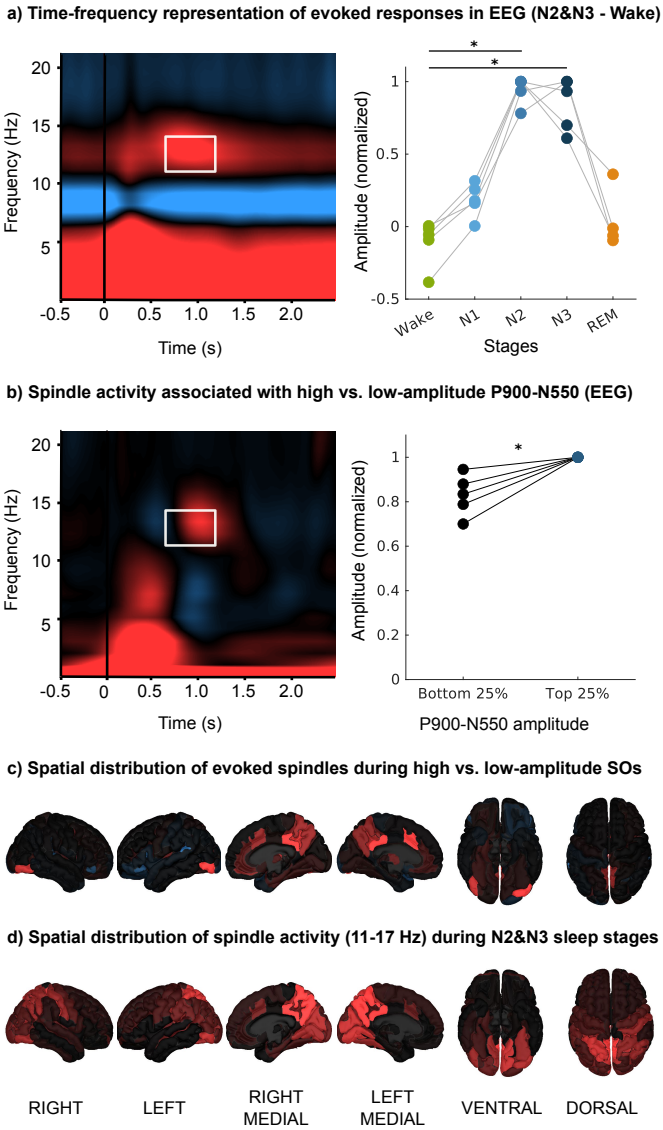

Fig. 5. Sound-evoked sleep spindles in EEG (Cz). a) The time-frequency plot averaged across all subjects (left) shows increased spindle power in N2&N3 sleep 0.6 to 1.2 s after sound onset in a frequency band of 11 to 14 Hz (white rectangle). Spindle power in that frequency range as compared with spindle power in the pre-stimulus baseline (-0.6 to 0 ms) is shown at right. Asterisks denote significant differences between Wake and N2 & N3. b) Spindle activity is positively related to evoked N550-P900 complex amplitude. When epochs are divided according to the strength of the slow oscillation that they produce (i.e., Top vs. Bottom 25%), stronger spindle power is observed to be coincident with stronger N550-P900 complexes in the EEG time-frequency plot (left), and extracted values are higher across subjects (right). Asterisks indicate a significant difference between Wake and deeper sleep conditions (Wilcoxon signed-rank test on the means; $p < .05$). c) The topography of spindle power differences (in MEG) according to evoked N550-P900 complex strength (Top vs. Bottom 25% of N550-P900 complexes averaged across subjects) shows increased activity in thalamus and frontal midline structures coincident with stronger N550-P900 complexes. d) The topography of spindle power in the 11-17 Hz range across all N2 & N3 sleep epochs, for comparison.

Temporal evolution of auditory evoked responses in MEG source space. To explore the time course of neural events in specific brain regions, we extracted time series from cortical regions thought to be involved in the generation of cortical auditory evoked responses (AC and OFC) as well as other sensory regions used as controls (S1/M1 and V1). We averaged the extracted signals across trials and hemispheres according to sleep stage and measured the amplitude of activity during specific time windows (P200 between 165 and 205ms, and the N550-P900 complex), for each subject (see Figure 6). We observed peaks of activity in the AC and OFC at about 100 and 200 ms after sound onset (P100, P200), and troughs in OFC and AC occurring around

350-550 ms post-onset (N350, N550). There is some evidence of brain activity in V1, M1 and S1 within 300 ms of sound onset, but peaks appeared delayed or indistinct with respect to AC and EEG.

We then conducted LME analyses on P200 amplitude, using subjects as a random effect to compare amplitude between Wake and N2&N3. We removed outliers from each ROI by excluding values based on thresholds defined as 1.5 times the interquartile range (i.e., below Q1 and above Q3). The mean percentage of retained epochs across subjects was 90.4% (SD = 5.90). Using a null-intercept linear mixed effect model we found that only AC (β = 10.14, SE = 0.48, z(5.63) = 21.14, p < .0001) and the OFC (β = 2.81, SE = 0.48, z(5.6707) = 5.84, p = .001) across Condition (Sleep and Wake merged) are statistically greater than zero, as suggested by Figure 6. We then focused on these two regions of interest to assess the impact of sleep state (Condition). Using a new linear mixed effects model with ROI as fixed effect and Subject as random effect (Amplitude $\sim$ 1+ ROI +(1|Subject)), we found a main effect of ROI, meaning that they are significantly different across Conditions (F(1,76138) = 832.77, p < .0001). Adding the interaction between Condition and ROI improved model fit (Amplitude $\sim$ 1+ ROI + Condition + ROI * Condition + (1|Subject)) as compared with fixed effects of ROI and Condition only ($\chi^2(1)$ = 29.87, p < .0001). We do not find a main effect of Condition (Wake, Sleep on P200 amplitude across ROIs (F(1, 72083) = 0.18, p = 0.67) but there is a main effect of ROI (F(1, 76138) = 832.77, p < .0001) as in the ROI-only model, with AC estimated mean amplitude (M = 10.17, SE = 1.08) being higher than OFC estimated mean amplitude (M = 2.78, SE = 1.08). There is a main effect of interaction between ROI and Condition (F(1, 76134) = 29.46, p < .0001), meaning that the ROIs do not behave similarly across wake and sleep states. Post-hoc analysis using estimated means showed that AC amplitude in Sleep is lower than in Wake (Sleep-Wake difference, M = -1.80, SE = 0.44, p = .0003) and that OFC amplitude is higher in Sleep than Wake (Sleep-Wake difference, M = 1.52, SE = 0.46, p = .0052). On an exploratory basis, we also tested Hemisphere (Left and Right) as a fixed effect, as compared with the null model ($\chi^2(1)$ = 71.49 , p < .0001). The results suggest that on average across Condition and ROI, P200 amplitude is greater in the left hemisphere than in the right hemisphere (Left-Right difference, M = 2.17, SE = 0.26, p < .0001). The emergence of an auditory response in OFC woud suggest the involvement of the non-lemniscal pathway as suggested by Model 3 and 4.

Next, we conducted LME analyses to investigate the elicited N550-P900 complex amplitude, testing our hypothesis that change in amplitude would be greater in Sleep than in Wake (as seen in the time series average, see Supplementary Figure 1). We removed outliers from each ROI using the same process as defined in the P200 analysis. The mean percentage of retained epochs across subjects was 89.4% (SD = 6.18). First, using a null-intercept linear mixed effect model we found that only the OFC across Condition (Sleep and Wake merged) is statistically greater than 0 (β = 1.15, SE = 0.26, z(8.1545) = 4.5, p = .002). Focusing on the OFC only (Amplitude $\sim$ 1 + Condition +(1|Subject)), we found a main effect of Condition (F(1, 3946.3) = 20.7, p < .0001). Post-hoc analysis using estimated means showed that OFC amplitude in Sleep is higher than in Wake (Sleep-Wake difference, M = 2.17, SE = 0.48, p < .0001). On an exploratory basis, we also tested Hemisphere (Left and Right) as a fixed effect, as compared with the null model ($\chi^2(1)$ = 9.66, p = .002). The results suggest that on average across Condition, elicited N550-P900 complex amplitude is greater in the left OFC than in the right OFC (Left-Right difference, M = 1.19, SE = 0.38, p = .002). The absence of N550-P900 complex in V1, M1 and S1 does not suggest the existence of a global generation of slow evoked response by the arousal system as suggested by Model 3. The biggest change in late components occurs in the OFC, in-line with models that propose that the SO generator is primarily in orbitofrontal regions (Models 2 and 4).

These data suggest that regional contributions to the global cortical ERP differ by brain state (Wake vs. Sleep), with earlier components (as measured via the amplitude of P200) being associated mainly with activity in the auditory cortex and the OFC, and later components (as measured via the amplitude of the N550-P900 complex) linked to higher change in activity solely in the OFC. For further analyses of evoked oscillations and functional connectivity, we focused on the OFC and AC regions, as they seem most affected by brain state and are relevant to our SO generation models (Figure 1).

Functional connectivity between auditory and orbitofrontal cortex following sound stimulation in sleep. The results of the connectivity analysis are represented schematically in Figure 7. LME analyses were conducted to investigate functional connectivity between AC and OFC in successive non-overlapping frequency bands (0.1-1.5 Hz, 2-4 Hz, 5-7 Hz, 8-10 Hz, 11-17 Hz, 18-29 Hz, 30-58 Hz). Functional connectivity was computed separately in each hemisphere. Outliers were removed using the same process defined above. The mean percentage of retained epochs across subjects was similar in both hemispheres (Left,

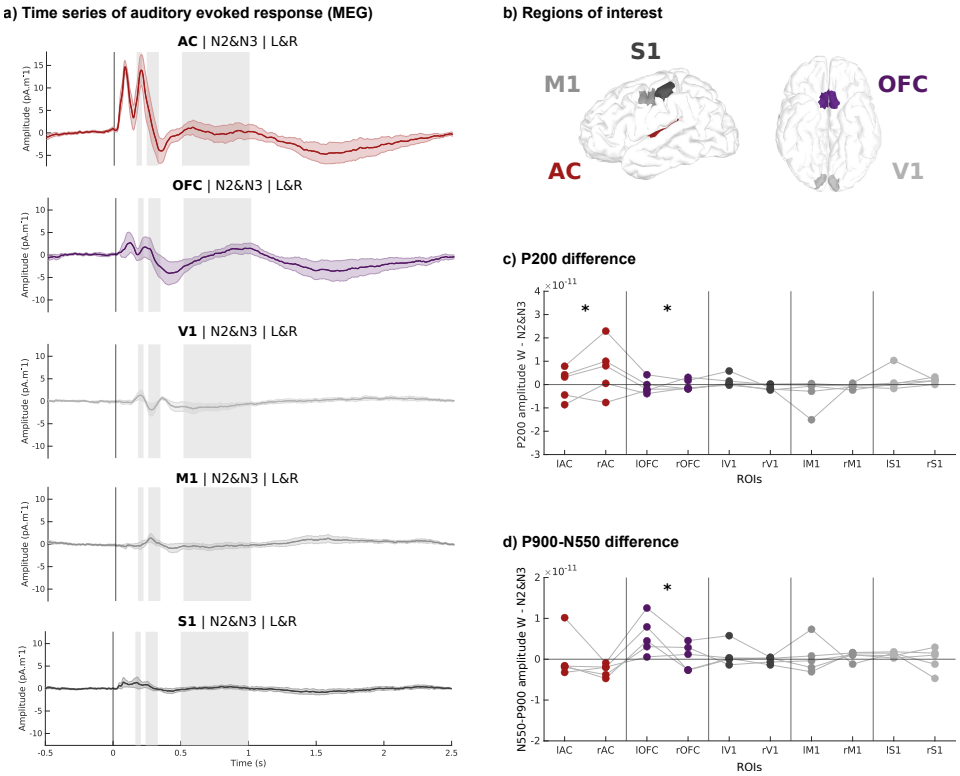

Fig. 6. Evoked responses in N2 & N3. a)Time series, averaged across subjects and hemispheres, for each region of interest. b) Schematic view of regions of interest. c) P200 amplitude differences between Wake and N2 & N3 for each region of interest and each hemisphere. d) N550-P900 complex amplitude differences between Wake and N2 & N3 for each region of interest and each hemisphere. Asterisks denote significant differences between Wake and N2 & N3 ($p < .01$).

M = 98.7% SD = 0.9 and Right, M = 98.8%, SD = 0.6).

In both the right and left hemisphere, dPTE values were significantly lower than 0 in the 0.1-1.5 Hz frequency band, indicating connectivity from OFC to AC (Left: β = -2.22e-02, SE = 6.89e-04, t(5.99) = -32.24, $p < .0001$; Right: β = -2.46e-02, SE = 9.54e-04, t(5.53) = -25.77, $p < .0001$). In the higher frequency ranges, the pattern is reversed, with modest but statistically significant directional connectivity from AC to OFC (between 5 Hz and 29 Hz on the left and similarly for the right side except that 11-17 Hz bin was non-significant; see Figure 7 for trends and Supplementary Table 1 and 2 for numerical values). Together these results provide evidence for an OFC to AC directed connectivity in the slow oscillation frequency band where the N550-P900 component would be generating in the OFC before propagating to other cortical areas, including the AC (favouring Models 2 and 4).

Effect of regionally-specific cortical states on responses.

Comparison of EEG and regional extracted time series during EEG up-states. Closed-loop auditory stimulation usually targets EEG up-states (i.e., peaks in the slow frequency range of about 0.1-2.0 Hz). To compare the EEG recordings to the signals extracted from the AC and OFC ROIs, we first detected slow oscillation up-states in the EEG signal and defined 4-second windows ($+/-2$ s around each detected peak). We then computed (zero phase lag) correlations between the EEG and each of the four source-space MEG time series (rAC, lAC, rOFC and lOFC). The average time series for EEG and the ROIs are presented in Figure 8(top); when the EEG is in an up-state, AC and OFC also generally seem to be in an up-state.

We conducted LME analyses using subjects as a random effect to identify which ROI's activity correlates most with scalp EEG activity recorded at Cz, a commonly used electrode placement in SO-CLAS paradigms. Due to the intrinsic property of correlation values to be bounded between -1 and 1, no outlier removal process was implemented. Using a null-intercept linear mixed effect model with ROI as fixed effect and Subject as random effect, we found that correlations of both AC (β = 0.11, SE = 0.02, t(5.02) = 4.87, p = .005) and OFC (β = 0.08, SE = 0.02, t(5.02)= 3.35, p = .02) activity with EEG activity were

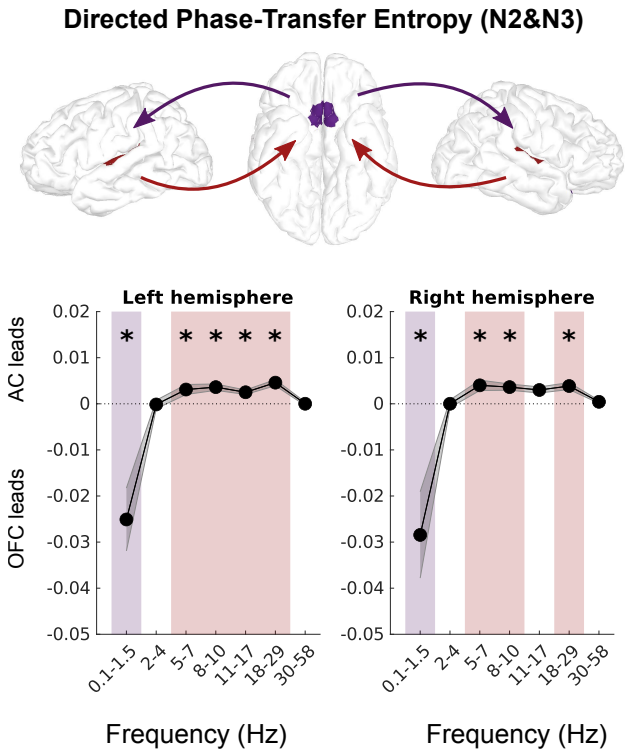

Fig. 7. Functional connectivity (directed phase-transfer entropy) between auditory (red) and orbitofrontal (purple) cortices. Frequency bands that have significant directed connectivity are shaded in the colour of the leading region of interest. Asterisks denote significance ($p < .05$).

significantly greater than 0 across subjects. Using a new linear mixed-effect model to compare ROI (Correlation $\sim$ 1 + ROI + (1 | Subject), we found a main effect of ROI. The EEG-OFC correlation was significantly lower than EEG-AC correlation (β = -3.49e-02, SE = 2.68e-03, t(6.590e+04) = -13.03, p < .0001). We also further explored the lateralization effect noted in the previous analyses. Adding Hemisphere as a second fixed effect increased model fit ($\chi^2(1)$ = 483.62, p < .0001), with overall EEG activity being more correlated with ROI activity in the left hemisphere (F(1, 65899) = 485.40, p < .0001). This result is coherent with the previously observed dominance of the left hemisphere in other analysis.

Comparison of EEG and regional extracted phases during EEG peak. To further explore the relationship between single-channel EEG and regional brain activity, we calculated the instantaneous phase of the extracted ROI signals at the time EEG up-states were detected. Because phase angles are bounded between $-\pi$ and π rad, no outlier removal process was implemented. As shown in Figure 8, phase distribution from the four key regions of interest were far more dispersed than in the EEG, and only a small percentage of trials were aligned with a simultaneous EEG up-state (phase difference between EEG and ROI $+/-\frac{\pi}{6}rad$; lAC M = 11.5 % SD = 0.9; rAC M = 12.7 %, SD = 1.6; lOFC M = 13.7 %, SD = 4.6; rOFC M = 9.5 %, SD = 1.7). We then computed F-scores to compare the variance of the EEG distribution with that of each ROI. The variance of phase distribution (i.e., dispersion) of each ROI was significantly greater than that of EEG (F(16487) = 0.33, p < .001), lAC phase distribution (F(16487) = 0.33, p < .0001), lOFC phase distribution (F(16487) = 0.26, p < .001) and rOFC phase distribution (F(16487) = 0.31, p < .001). These results indicate that up-states as determined by single-channel (Cz) EEG only partially coincide with local up-states in key cortical regions.

Comparison of EEG evoked responses as a function of regional tissue state. To identify the impact of regionally-specific cortical tissue excitability level on the evoked brain response, we detected up-states and down-states of slow activity (0.1 - 2.0 Hz) in each key region of interest. We then computed the amplitude of the elicited N550-P900 complex and spindle activity across condition (Up-state vs. Down-state). We focused on evoked responses as measured in EEG for comparability with previous literature, and because evoked responses may not be highly localized. Concerning the elicited N550-P900 complex amplitude, we conducted LME analyses to investigate the impact of up and down-states of both the OFC and the AC.

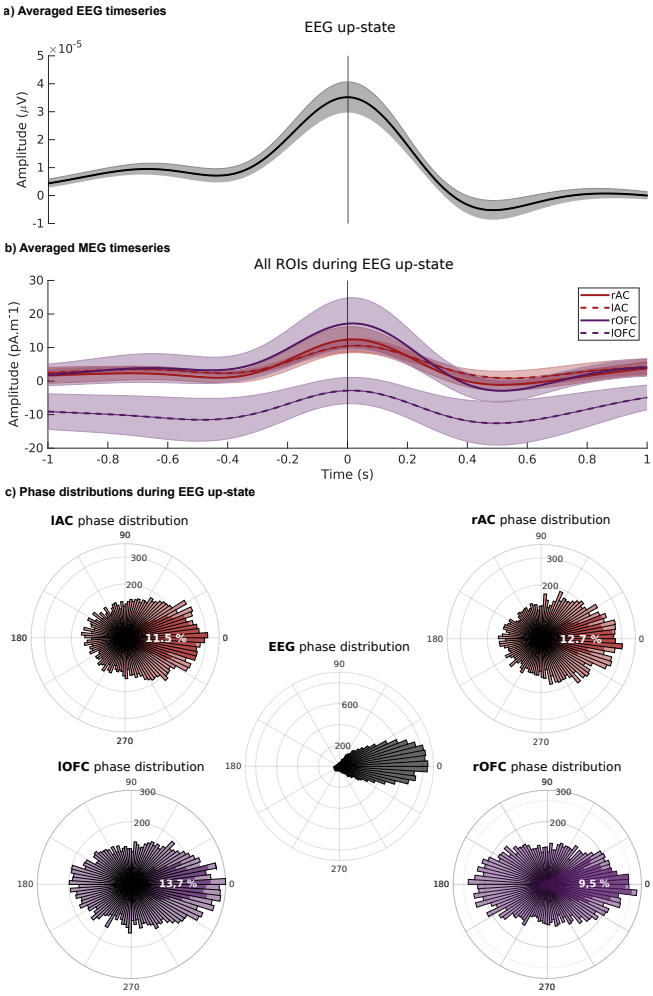

Fig. 8. Comparison of EEG and MEG activity from auditory (lAC, rAC) and orbitofrontal (lOFC, rOFC) regions of interest. a) EEG averages across subjects, aligned by up-state as detected in EEG. b) MEG ROI averages across subjects, aligned by up-state as detected in EEG. c) Polar histograms indicating phase distribution of EEG and ROIs during up-state as detected in EEG. The percentage of trials with aligned phase between each ROI and EEG is indicated schematically in darker shading, and numerically in superimposed white text ($+/-\frac{\pi}{6}rad$). Shaded bars indicate SEM in a) and b).

Including Condition (Up-state vs. Down-state) as a fixed effect in a linear mixed-effect model increased model fit (Amplitude $\sim$ 1 + Condition +(1|Subject)) as compared to a null intercept-only model ($\chi^2(1) = 4.08$, p = .043), indicating across ROIs, stimulation occurring during an up-state elicited a larger-amplitude N550-P900 complex as observed in EEG, compared to down-states. Adding the interaction of ROI and Condition (Amplitude $\sim$ 1 + Condition*ROI +(1|Subject)) resulted in a better-fitting model ($\chi^2(2) = 15.34$, p = .0005). Post-hoc analysis using estimated means showed that tissue state in the OFC was critical to the generation of N550-P900 complex (OFC: Up vs. Down-state difference, M = 8.43, SE = 2.01, p = .0002), whereas tissues state in the AC did not significantly affect N550-P900 complex amplitude as measured in EEG (AC: Up vs. Down-state difference, M = -2.56, SE = 1.96, p = 0.56). On an exploratory basis, we also tested Hemisphere (Left and Right) as a fixed effect, as compared with the previous model ($\chi^2(1) = 0.03$, p = 0.86). The comparison suggests that Hemisphere does not account for more variance in the data, meaning that differences in tissue state across left and right OFC does not clearly impact the N550-P900 complex as observed in EEG. These results provide additional evidence for a critical role of the OFC in the SO generation. Auditory cortex excitability state instead does not seem to matter, further implicating the non-lemniscal auditory pathway in the CLAS effect and decreasing the likelihood of Model 2, in which the auditory information passes first to the AC via the lemniscal pathway. Together, these results are best explained by Model 4.

A similar analysis was used to investigate the effect of ROI cortical state on the increase in spindle activity. For each epoch, root mean squared values of the EEG sigma filtered in the previously defined frequency band of interest (11-14 Hz) was computed in the time windows of interest (0.6 to 1.2 s) post-stimulation, as well as before stimulation to serve as baseline (-0.6 to 0 s).

We first investigated the conditions affecting the production of spindle power by auditory stimulation, using zero-intercept models (Spindle Power Change $\sim$ 0 + ROI + (1 | Subject) and Spindle Power Change $\sim$ 0 + Condition + (1 | Subject)). In each ROI, across Condition (Up and Down-state merged), auditory stimulation statistically increased spindle power as compared to a pre-stimulation baseline (AC, $\beta = 0.51$, SE = 0.19, t(5.3522) = 2.74, p = .04 and OFC, $\beta = 0.55$, SE = 0.19, t(5.42) = 2.82, p = .04) Collapsing instead across ROIs, auditory stimulation statistically increased spindle power in Up-states ($\beta = 0.58$, SE = 0.18, t(5.31) = 3.16, p = .02), but not Down-states ($\beta = 0.44$, SE = 0.19, t(5.51) = 2.35, p = .06).

To compare between ROIs, we used a LME with Subjects as random effect (Spindle Power Change $\sim$ 1 + Condition + (1 | Subject)). We find a main effect of Condition (tissue excitability as measured with ROI Up and Down-state, (F(5716) = 4.14, p = .04)) with Up-state stimulation eliciting greater spindle power, as measured in EEG, than Down-state stimulation. Adding the interaction between ROI and Condition (Amplitude $\sim$ 1 + Condition*ROI +(1|Subject)) did not improve model fit ($\chi^2(2) = 2.18$, p = 0.34).

For completeness, we also tested Hemisphere (Left and Right) as a fixed effect (Spindle Power Change $\sim$ 1 + Condition + Hemisphere + (1 | Subject)), as compared with the Condition-only model ($\chi^2(1) = 1.69$, p = 0.19). The comparison suggests that Hemisphere does not account for additional variance in the data, meaning that differences in tissue state across left and right OFC do not clearly impact spindle generation.

Discussion

Evaluating evidence for SO generation models. Understanding the neurophysiology of closed-loop auditory stimulation requires identification of the origin of auditory evoked brain responses during sleep. The main goal of this work was to define potential mechanistic models based on previous literature (Figure 1) and to evaluate their ability to explain spatially-resolved evoked brain responses in the sleeping brain, including slow oscillations and sleep spindles, and by association, the beneficial effects on memory consolidation that have been reported in literature (Choi et al., 2020, Harrington and Cairney, 2021, Nasr et al., 2022), as well as other sleep-related physiological functions (Besedovsky et al., 2017, Kelley et al., 2022).

According to the first potential model we described (Figure 1), slow oscillations would be generated locally within the auditory cortex upon the arrival of sound information through lemniscal auditory pathways at primary auditory cortex in the superior temporal gyrus. If this were the case, we would expect SOs to occur first in this region before propagating to subsequent cortical regions. Although we do observe clear evoked auditory responses in sleep that are similar to those in the Wake state up to and including 200 ms (P200), the evoked slow oscillations appear strongest in the orbitofrontal region (Figure 4, 6). Additional evidence against this model comes from the functional connectivity analysis (see Figure 7), which shows that in the

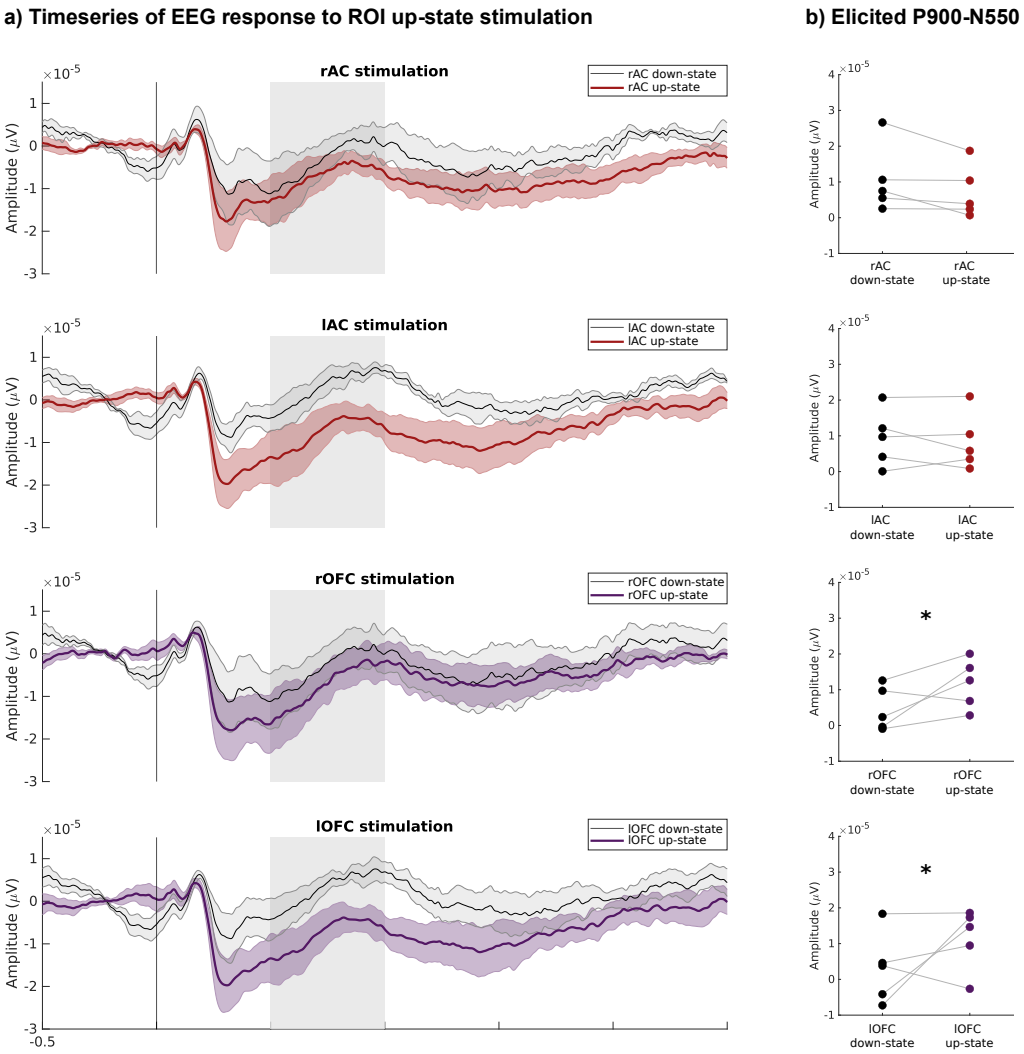

Fig. 9. Evoked responses in EEG divided according to the excitability state of local tissue in auditory (rAC, lAC), and orbitofrontal (rOFC and lOFC) regions of interest. a) Comparison of the EEG time series for up-state and down-state stimulation compared with MEG time series extracted from ROIs. b) Mean N550-P900 complex amplitude for each ROI in each condition. c) Mean increase in spindle activity for each ROI in each condition. Each subject is represented by its mean. Asterisks denote significant differences between Peak and Trough stimulation using LME statistical models (* = $p < .001$).

slow oscillation frequency range (0.5-1.5 Hz), information flows in the reverse direction; from OFC to AC (replicated in both left and right hemispheres). These findings align with previous reports that the primary generator of (endogenous) SOs is found in ventral frontal areas (Morgan et al., 2021). In the second of the proposed models (Model 2 in Figure 1), sound information would arrive at the auditory cortex via primary auditory pathways and would then be passed forward to frontal regions, which would generate slow oscillations. This model relies on the progression of auditory information from auditory cortex to ventral frontal regions. Although we did observe connectivity from AC to OFC in higher frequencies (i.e., $>$ 5Hz), it was of very low strength. The majority of the energy in auditory evoked responses is captured in the $<$ 5 Hz frequency range (confirmed by applying filters with different band pass limits). Although it cannot entirely be ruled out on the basis of the present analysis, it seems unlikely that the modest AC to OFC connectivity we observed in high frequency ranges is the trigger for SO generation in OFC. Moreover, the observation that SOs are more likely to be generated when tissue in OFC is in an up-state at the time of stimulation as compared with AC, suggests that the non-lemniscal auditory pathway is most relevant for the CLAS effect.

Models 3 and 4 consider the involvement of the non-lemniscal pathway as a potential mechanism for auditory evoked responses as suggested by Bellesi et al. (2014). They hypothesized that CLAS is likely mediated by the activation of the non-lemniscal ascending auditory pathway, which projects broadly to association areas including frontal regions and secondary auditory areas (Bellesi et al., 2014, Kjaerby et al., 2022). They proposed that the modulation of noradrenaline levels by the locus coeruleus is critical for the generation of N550-P900 complexes, and that low noradrenaline levels might be a necessary factor for the emergence of an evoked N550-P900 complex, whereas elevated levels of noradrenaline would result in arousal.

In Model 3, a signal generated in the arousal network via interactions with the non-lemniscal auditory system in the brainstem and thalamus would cause changes to neural activity in widespread areas, and generate slow oscillations throughout the cortex. Although this domain-generality is plausible from work showing that visual, tactile, and auditory stimulation can all generate slow oscillations (Riedner et al., 2011), we do not find that slow oscillations are generated via auditory stimulation in any of the other selected cortical regions (V1, M1, S1), nor do we observe activity within the whole brain maps during the evoked N550-P900 complex (Figures 4 and 6). Moreover, the significant functional connectivity in the slow wave frequency band from OFC to AC would not be observed if both the OFC and the AC were generators of slow oscillation receiving simultaneous stimulation from a common source (Figure 7).

Finally, in Model 4, the general arousal system is implicated, but it is the ventral frontal regions that generate slow oscillations. This model is supported by the finding that frontal and ventral regions show the strongest SOs, as well as the functional connectivity analysis, which shows that information flows from OFC to AC bilaterally in the slow wave frequency range.

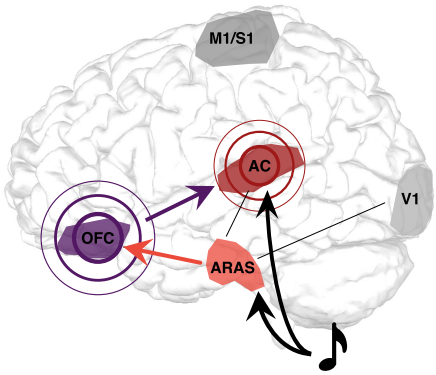

Fig. 10. Proposed model concerning the generation of slow oscillations in sleep by auditory stimulation. The evidence presented in this work suggests a cross between models 1 and 4 described in Figure 1, in which neural activity stimulated by a sound impulse ascends in parallel to the auditory cortex via auditory pathways, where it generates evoked responses ($<$ 300 ms) typical of auditory stimulation in other states, and also ascends via modality-general arousal systems to frontal regions, where more pronounced SOs are generated that then propagate to other brain regions.

Based on the quantitative measures of evoked responses (see Figure 6), the connectivity pattern observed (see Figure 7) as well as the sensitivity to auditory stimulation (see Figure 9), we propose a fifth model suggesting the ventral limbic areas (orbitofrontal cortex) as the primary generator of the evoked N550-P900 complex (Figure 10). This final model is a combination

of Model 1 and Model 4 (see Figure 1), in which auditory information is processed in a parallel fashion by the lemniscal and non-lemniscal pathways. Early components of the evoked response in scalp EEG originate in both the auditory cortices, likely through the lemniscal pathway and the OFC. Later components of the observed brain response in the EEG are proposed to come from the OFC upon its activation through the non-lemniscal pathway (as suggested by the presence of auditory brain response in the OFC visible in Figure 6). The elicited N550-P900 complex would then propagate elsewhere in the cortex (including AC).

Evoking sleep spindles. Although the definition of the models focused primarily on the neurophysiology of closed-loop auditory stimulation on slow and high amplitude evoked responses, we also investigated the generation of spindles evoked by auditory stimulation, due to their importance in sleep's memory consolidation function and in the CLAS effect (Fernandez and Lüthi, 2020, Ngo et al., 2013). Previous research focused on the increase in spindle activity when auditory stimulation is time-locked to the peak of the targeted slow oscillation (Ngo et al., 2013). However, a study by (Sato et al., 2007) showed that non-arousing stimulation using different sensory modalities (somatosensory, auditory, or visual) during stage N2 sleep also induced an increase in spindle activity in related sensory cortical areas. Spindle generation is often not reported in sleep studies focusing on ERPs (Colrain and Campbell, 2007), as they are not precisely time-locked to stimulation events and disappear when independent trials are averaged (in the time domain). By using time-frequency analyses and analyzing sigma power within specific time windows following stimulation, we replicated the observation that sleep spindles are elicited in N2 and N3 sleep (Ngo et al., 2013). Furthermore, we showed that spindle amplitude was bigger in trials that successfully generated higher N550-P900 complexes. MEG topographies of these evoked spindles show a pattern of activation in medial and dorsal brain regions including the precuneus, which is similar to the pattern of activity in the spindle frequency range throughout N2 and N3 sleep stages (see Figure 5).

Interestingly, even if their presence is linked to the amplitude of the evoked N550-P900 complex (as seen the Figure 5 b), the elicited spindle activity does not seem to depend on the local activity of the key regions of interest we selected for our analysis; both AC and OFC up-state stimulation induces an increase in spindle activity which is greater than down-state stimulation. We can hypothesize that even if the spindle and the N550-P900 generation mechanisms are intertwined, they are not identical. Other factors, potentially the state of activity in other regions, might modulate the degree of spindle activity generated.

Improving the effectiveness of CLAS. While the effect of CLAS on physiology and memory largely replicates across studies (Choi et al., 2020, Harrington and Cairney, 2021, Wunderlin et al., 2021), there are inter-individual differences in the effectiveness of non-invasive brain stimulation (Guerra et al., 2020, Ziemann and Siebner, 2015), and effectiveness appears to change over the lifespan (Schneider et al., 2020). Attempts have therefore been made to identify the best timing for CLAS with respect to tissue excitability state as detected in a single EEG channel (in younger and older populations) (Navarrete et al., 2020), and to target local SOs in different brain regions using the spatial information that is available in multichannel EEG data (Ruch et al., 2022). Our investigation of phase in EEG and MEG makes several contributions to this area. Notably, we found that although EEG up-states detected in single channel over frontal areas does on average correlate with up-states in both AC and OFC (Figure 8a), only $\sim$10-15% of slow oscillation up-states detected in EEG correspond to up-states in each of these regions (Figure 8b). As the state of the OFC is most critical to successful generation of N550-P900 complexes and their associated spindles (Figure 9), which both play important roles in memory consolidation, particularly when they are coupled (Hahn et al., 2020, Mikutta et al., 2019, Muehlroth et al., 2019), it is likely that increased efficiency and reliability of CLAS can be obtained by selectively targeting up-states in ventral frontal regions. This goal could be achieved by detecting patterns in multichannel EEG (e.g., (Ruch et al., 2022)), and/or machine learning-approaches that can detect fine-grained signatures on one or several channels that stimulate the brain with optimal timing (e.g., Valenchon et al. (2022)), and perhaps adapt detection parameters in real time to an individual's idiosyncratic neural signals. These ideas are in alignment with the emerging concepts of 'precision neuroimaging' and 'person specific methods', in which reliable individual differences in brain activation or connectivity are studied to understand (and sometimes make use of) individual differences in brain function and behaviour Michon et al. (2022).

Limitations and next steps. One limitation of our study is that due to the nature of our study design, we were not able to distinguish between elicited (evoked) and endogenous brain activity. The topographies of endogenous SOs and spindles

offered in Figures 3b and 5d for visual comparison with the evoked activity are therefore approximations that are strongly weighted towards endogenous activity, but nonetheless also capture evoked activity. Comparing periods of evoked oscillations in stimulated sleep and endogenous oscillations in unstimulated sleep in the same individuals would allow for a more rigorous evaluation of the similarities and differences in slow oscillations and spindles generated by sound (which was not an aim of the present work). The overnight design allowed us to record data in all sleep stages and have large numbers of trials in both N2 and N3 sleep, which is difficult to achieve in a nap design. Our LME-based statistical approach allowed us investigate our research questions, but our design does not allow us to account for the range of human variability in brain responses to sound in sleep. It would be interesting to explore individual differences across populations and over the lifespan, which would require a larger sample size. This research direction could help to explain why sensitivity to CLAS differs between individuals (Guerra et al., 2020, Ziemann and Siebner, 2015) and in older adults (Navarrete et al., 2020). Several of our analyses suggest a leftward lateralization in OFC involvement. We caution against overinterpreting these findings, as hemispheric differences in brain folding and ROI placement can affect the strength of observed signals in MEG source space; however, other studies using EEG have also found that low frequency oscillations in ventral limbic areas are more frequent on the left side (Achermann et al., 2001, Morgan et al., 2021), suggesting that a more focused analysis of lateralization may be an interesting area for future work. Finally, we opted to use standard surface-based cortical source localization models. Previous work has demonstrated that brain signals associated with information in the auditory lemniscal pathway can be extracted using MEG source space volume models (Coffey et al., 2016); however, signals extracted from these models are more difficult to work with and their use with functional connectivity metrics has not been validated. As MEG modelling and connectivity techniques develop, it may be possible to explore the involvement of brainstem regions and more directly test the involvement of the ARAS in brainstem-OFC interactions, to further refine models of SO generation.

Conclusion

In summary, our data suggest a crucial orbitofrontal contribution to the auditory-evoked N550-P900 complex that underlies the effect of closed-loop auditory stimulation on physiology and memory. Previous research mainly detected high states of excitability based on single channel scalp EEG, assuming that activity over frontal regions represents a global up-state. Our results suggest that targeting up-states in ventral frontal regions has potential to improve the effectiveness of CLAS. Clarifying how sound stimulates the brain has important implications for making causal manipulation tools like CLAS more effective in fundamental research and potential clinical applications.

Conflict of interest. The authors declare having no conflicts of interest.

Data availability statement. The raw MEG and EEG sleep recordings are accessible via the OMEGA open MEG archive (Niso et al., 2016). All extracted values used for statististical analyses are available on the Open Science Framework website (https://osf.io/afv9g/?view_only=24576c983b8941b1b429e18b42e17061).

Author contributions

Credit roles: Hugo Jourde: Methodology, Formal analysis, Writing - Original Draft, Writing - Review & Editing, Visualization. Raphaëlle Merlo and Meredith Rowe: Data collection, Writing - Review & Editing. Mary Brooks: Writing - Original Draft, Writing - Review & Editing. Emily Coffey: Conceptualization, Methodology, Formal analysis, Data Curation, Writing - Original Draft, Writing - Review & Editing, Visualization, Supervision, Project administration, Funding acquisition.

Acknowledgements

The authors would like to thank Sylvain Baillet and Mark Lalancette for assistance with MEG technical matters, Robert Zatorre for assistance with funding acquisition and consultation concerning results, Alexander Albury and Charlotte Emma Moore for help with statistical modelling, Marie-Anick Savard and Anita Paas for helpful comments on the manuscript, Alix Noly-Gandon for helping with several data recordings and confirming the sleep scoring, and lab members for general support. This work was

financially supported by a Natural Sciences and Engineering Research Council of Canada (NSERC) Discovery grant, a grant from the Fonds de recherche du Québec – Nature et technologies (FRQNT), the 'Healthy Brains for Healthy Lives' Canada First Research Excellence Fund (CFREF) at McGill University, and a Concordia (New Scholar) Research Chair in 'Sleep and Sound' to EBJC. HRJ was supported by a Graduate Scholar Stipend from the Centre for Research on Brain, Language and Music.

Bibliography

P. Achermann, L. A. Finelli, and A. A. Borbély. Unihemispheric enhancement of delta power in human frontal sleep eeg by prolonged wakefulness. *Brain research*, 913(2):220–223, 2001.

J. W. Antony, L. Piloto, M. Wang, P. Pacheco, K. A. Norman, and K. A. Paller. Sleep spindle refractoriness segregates periods of memory reactivation. *Current Biology*, 28(11):1736–1743, 2018.

J. W. Antony, M. Schönauer, B. P. Staresina, and S. A. Cairney. Sleep spindles and memory reprocessing. *Trends in neurosciences*, 42(1):1–3, 2019.

J. W. Antony, H.-V. V. Ngo, T. O. Bergmann, and B. Rasch. Real-time, closed-loop, or open-loop stimulation? navigating a terminological jungle. *Journal of Sleep Research*, page e13755, 2022.

S. Baillet. Magnetoencephalography for brain electrophysiology and imaging. *Nature neuroscience*, 20(3):327–339, 2017.

S. Baillet, J. C. Mosher, and R. M. Leahy. Electromagnetic brain mapping. *IEEE Signal processing magazine*, 18(6):14–30, 2001.

D. H. Baker, G. Vilidaite, F. A. Lygo, A. K. Smith, T. R. Flack, A. D. Gouws, and T. J. Andrews. Power contours: Optimising sample size and precision in experimental psychology and human neuroscience. *Psychological methods*, 26(3):295, 2021.

C. Bastien and K. Campbell. The evoked k-complex: all-or-none phenomenon? *Sleep*, 15(3):236–245, 1992.

C. H. Bastien, K. E. Crowley, and I. M. Colrain. Evoked potential components unique to non-rem sleep: relationship to evoked k-complexes and vertex sharp waves. *International Journal of Psychophysiology*, 46(3):257–274, 2002.

D. Bates, M. Mächler, B. Bolker, and S. Walker. Fitting linear mixed-effects models using lme4. *Journal of Statistical Software*, 67(1):1–48, 2015. doi: 10.18637/jss.v067.i01.

M. Bellesi, B. A. Riedner, G. N. Garcia-Molina, C. Cirelli, and G. Tononi. Enhancement of sleep slow waves: underlying mechanisms and practical consequences. *Frontiers in systems neuroscience*, 8: 208, 2014.

L. Besedovsky, H.-V. V. Ngo, S. Dimitrov, C. Gassenmaier, R. Lehmann, and J. Born. Auditory closed-loop stimulation of eeg slow oscillations strengthens sleep and signs of its immune-supportive function. *Nature communications*, 8(1):1–8, 2017.

W. Blanco, C. M. Pereira, V. R. Cota, A. C. Souza, C. Rennó-Costa, S. Santos, G. Dias, A. M. Guerreiro, A. B. Tort, A. D. Neto, et al. Synaptic homeostasis and restructuring across the sleep-wake cycle. *PLoS computational biology*, 11(5):e1004241, 2015.

M. Brysbaert and M. Stevens. Power analysis and effect size in mixed effects models: A tutorial. *Journal of cognition*, 1(1), 2018.

D. J. Buysse, C. F. Reynolds III, T. H. Monk, S. R. Berman, and D. J. Kupfer. The pittsburgh sleep quality index: a new instrument for psychiatric practice and research. *Psychiatry research*, 28(2): 193–213, 1989.

K. Campbell et al. Event-related potentials as a measure of sleep disturbance: a tutorial review. *Noise and Health*, 12(47):137, 2010.

J. Carrier, I. Viens, G. Poirier, R. Robillard, M. Lafortune, G. Vandewalle, N. Martin, M. Barakat, J. Paquet, and D. Filipini. Sleep slow wave changes during the middle years of life. *European Journal of Neuroscience*, 33(4):758–766, 2011.

J. Choi, M. Kwon, and S. C. Jun. A systematic review of closed-loop feedback techniques in sleep studies—related issues and future directions. *Sensors*, 20(10):2770, 2020.

E. B. Coffey, S. C. Herholz, A. M. Chepesiuk, S. Baillet, and R. J. Zatorre. Cortical contributions to the auditory frequency-following response revealed by meg. *Nature communications*, 7(1):1–11, 2016.

E. B. Coffey, A. M. Chepesiuk, S. C. Herholz, S. Baillet, and R. J. Zatorre. Neural correlates of early sound encoding and their relationship to speech-in-noise perception. *Frontiers in neuroscience*, 11: 479, 2017.

E. B. Coffey, I. Arseneau-Bruneau, X. Zhang, S. Baillet, and R. J. Zatorre. Oscillatory entrainment of the frequency-following response in auditory cortical and subcortical structures. *Journal of Neuroscience*, 41(18):4073–4087, 2021.

I. M. Colrain and K. B. Campbell. The use of evoked potentials in sleep research. *Sleep medicine reviews*, 11(4):277–293, 2007.

R. Cox, A. C. Schapiro, D. S. Manoach, and R. Stickgold. Individual differences in frequency and topography of slow and fast sleep spindles. *Frontiers in human neuroscience*, 11:433, 2017.

T. T. Dang-Vu, M. Bonjean, M. Schabus, M. Boly, A. Darsaud, M. Desseilles, C. Degueldre, E. Balteau, C. Phillips, A. Luxen, et al. Interplay between spontaneous and induced brain activity during human non-rapid eye movement sleep. *Proceedings of the National Academy of Sciences*, 108(37):15438–15443, 2011.

C. Destrieux, B. Fischl, A. Dale, and E. Halgren. Automatic parcellation of human cortical gyri and sulci using standard anatomical nomenclature. *Neuroimage*, 53(1):1–15, 2010.

S. Diekelmann and J. Born. The memory function of sleep. *Nature Reviews Neuroscience*, 11(2):114–126, 2010.

T. Donoghue, M. Haller, E. J. Peterson, P. Varma, P. Sebastian, R. Gao, T. Noto, A. H. Lara, J. D. Wallis, R. T. Knight, et al. Parameterizing neural power spectra into periodic and aperiodic components. *Nature neuroscience*, 23(12):1655–1665, 2020.

L. M. Fernandez and A. Lüthi. Sleep spindles: mechanisms and functions. *Physiological reviews*, 100(2):805–868, 2020.

G. Girardeau and V. Lopes-Dos-Santos. Brain neural patterns and the memory function of sleep. *Science*, 374(6567):560–564, 2021.

R. J. Grissom and J. J. Kim. *Effect sizes for research: Univariate and multivariate applications.* Routledge, 2012.

J. Gross, S. Baillet, G. R. Barnes, R. N. Henson, A. Hillebrand, O. Jensen, K. Jerbi, V. Litvak, B. Maess, R. Oostenveld, et al. Good practice for conducting and reporting meg research. *Neuroimage*, 65: 349–363, 2013.

A. Guerra, V. López-Alonso, B. Cheeran, and A. Suppa. Solutions for managing variability in non-invasive brain stimulation studies. *Neuroscience letters*, 719:133332, 2020.

M. A. Hahn, D. Heib, M. Schabus, K. Hoedlmoser, and R. F. Helfrich. Slow oscillation-spindle coupling predicts enhanced memory formation from childhood to adolescence. *Elife*, 9:e53730, 2020.

P. Halász. The k-complex as a special reactive sleep slow wave–a theoretical update. *Sleep medicine reviews*, 29:34–40, 2016.

M. Hämäläinen. Mne software user's guide v2. 7. Technical report, MGH/HMS/MIT Athinoula A, 2009.

M. O. Harrington and S. A. Cairney. Sounding it out: Auditory stimulation and overnight memory processing. *Current Sleep Medicine Reports*, 7(3):112–119, 2021.

N. L. Hauglund, C. Pavan, and M. Nedergaard. Cleaning the sleeping brain–the potential restorative function of the glymphatic system. *Current Opinion in Physiology*, 15:1–6, 2020.

A. Hillebrand, P. Tewarie, E. Van Dellen, M. Yu, E. W. Carbo, L. Douw, A. A. Gouw, E. C. Van Straaten, and C. J. Stam. Direction of information flow in large-scale resting-state networks is frequency-dependent. *Proceedings of the National Academy of Sciences*, 113(14):3867–3872, 2016.

R. W. Homan, J. Herman, and P. Purdy. Cerebral location of international 10–20 system electrode placement. *Electroencephalography and clinical neurophysiology*, 66(4):376–382, 1987.

C. Iber. The aasm manual for the scoring of sleep and associated events: Rules. *Terminology and Technical Specification*, 2007.

O. Jaar, M. Pilon, J. Carrier, J. Montplaisir, and A. Zadra. Analysis of slow-wave activity and slow-wave oscillations prior to somnambulism. *Sleep*, 33(11):1511–1516, 2010.

D. H. Kelley, T. Bohr, P. G. Hjorth, S. C. Holst, S. Hrabětová, V. Kiviniemi, T. Lilius, I. Lundgaard, K.-A. Mardal, E. A. Martens, et al. The glymphatic system: Current understanding and modeling. *Iscience*, page 104987, 2022.

C. Kjaerby, M. Andersen, N. Hauglund, V. Untiet, C. Dall, B. Sigurdsson, F. Ding, J. Feng, Y. Li, P. Weikop, et al. Memory-enhancing properties of sleep depend on the oscillatory amplitude of norepinephrine. *Nature Neuroscience*, 25(8):1059–1070, 2022.

J. G. Klinzing, N. Niethard, and J. Born. Mechanisms of systems memory consolidation during sleep. *Nature neuroscience*, 22(10):1598–1610, 2019.

K. Lacourse, J. Delfrate, J. Beaudry, P. Peppard, and S. C. Warby. A sleep spindle detection algorithm that emulates human expert spindle scoring. *Journal of neuroscience methods*, 316:3–11, 2019.

V. Latreille, N. von Ellenrieder, L. Peter-Derex, F. Dubeau, J. Gotman, and B. Frauscher. The human k-complex: insights from combined scalp-intracranial eeg recordings. *Neuroimage*, 213:116748, 2020.

M. Laurino, D. Menicucci, A. Piarulli, F. Mastorci, R. Bedini, P. Allegrini, and A. Gemignani. Disentangling different functional roles of evoked k-complex components: mapping the sleeping brain while quenching sensory processing. *Neuroimage*, 86:433–445, 2014.

C. C. Lee. Exploring functions for the non-lemniscal auditory thalamus. *Frontiers in Neural Circuits*, 9:69, 2015.

R. V. Lenth. *emmeans: Estimated Marginal Means, aka Least-Squares Means*, 2022. URL https://CRAN.R-project.org/package=emmeans. R package version 1.8.2.

M. Lobier, F. Siebenhühner, S. Palva, and J. M. Palva. Phase transfer entropy: a novel phase-based measure for directed connectivity in networks coupled by oscillatory interactions. *Neuroimage*, 85: 853–872, 2014.

M. Massimini, R. Huber, F. Ferrarelli, S. Hill, and G. Tononi. The sleep slow oscillation as a traveling wave. *Journal of Neuroscience*, 24(31):6862–6870, 2004.

K. J. Michon, D. Khammash, M. Simmonite, A. M. Hamlin, and T. A. Polk. Person-specific and precision neuroimaging: Current methods and future directions. *Neuroimage*, page 119589, 2022.

C. Mikutta, B. Feige, J. G. Maier, E. Hertenstein, J. Holz, D. Riemann, and C. Nissen. Phase-amplitude coupling of sleep slow oscillatory and spindle activity correlates with overnight memory consolidation. *Journal of sleep research*, 28(6):e12835, 2019.

C. G. Moreira, C. R. Baumann, M. Scandella, S. I. Nemirovsky, S. Leach, R. Huber, and D. Noain. Closed-loop auditory stimulation method to modulate sleep slow waves and motor learning performance in rats. *Elife*, 10:e68043, 2021.

K. K. Morgan, E. Hathaway, M. Carson, M. Fernandez-Corazza, R. Shusterman, P. Luu, and D. M. Tucker. Focal limbic sources create the large slow oscillations of the eeg in human deep sleep. *Sleep Medicine*, 85:291–302, 2021.

B. E. Muehlroth, M. C. Sander, Y. Fandakova, T. H. Grandy, B. Rasch, Y. L. Shing, and M. Werkle-Bergner. Precise slow oscillation–spindle coupling promotes memory consolidation in younger and older adults. *Scientific reports*, 9(1):1–15, 2019.

K. Nasr, D. Haslacher, E. Dayan, N. Censor, L. G. Cohen, and S. R. Soekadar. Breaking the boundaries of interacting with the human brain using adaptive closed-loop stimulation. *Progress in Neurobiology*, page 102311, 2022.

M. Navarrete, J. Schneider, H.-V. V. Ngo, M. Valderrama, A. J. Casson, and P. A. Lewis. Examining the optimal timing for closed-loop auditory stimulation of slow-wave sleep in young and older adults. *Sleep*, 43(6):zsz315, 2020.

G. T. Neske. The slow oscillation in cortical and thalamic networks: mechanisms and functions. *Frontiers in neural circuits*, 9:88, 2016.

H.-V. V. Ngo, T. Martinetz, J. Born, and M. Mölle. Auditory closed-loop stimulation of the sleep slow oscillation enhances memory. *Neuron*, 78(3):545–553, 2013.

Y. Niiyama, R. Fujiwara, N. Satoh, and Y. Hishikawa. Endogenous components of event-related potential appearing during nrem stage 1 and rem sleep in man. *International Journal of Psychophysiology*, 17(2):165–174, 1994.

G. Niso, C. Rogers, J. T. Moreau, L.-Y. Chen, C. Madjar, S. Das, E. Bock, F. Tadel, A. C. Evans, P. Jolicoeur, et al. Omega: the open meg archive. *Neuroimage*, 124:1182–1187, 2016.

R. D. Ogilvie, I. A. Simons, R. H. Kuderian, T. MacDonald, and J. Rustenburg. Behavioral, event-related potential, and eeg/fft changes at sleep onset. *Psychophysiology*, 28(1):54–64, 1991.

J. Pinheiro and D. Bates. *Mixed-effects models in S and S-PLUS*. Springer science & business media, 2006.

B. Plakke and L. M. Romanski. Auditory connections and functions of prefrontal cortex. *Frontiers in neuroscience*, 8:199, 2014.

G. R. Poe, S. Foote, O. Eschenko, J. P. Johansen, S. Bouret, G. Aston-Jones, C. W. Harley, D. Manahan-Vaughan, D. Weinshenker, R. Valentino, et al. Locus coeruleus: a new look at the blue spot. *Nature Reviews Neuroscience*, 21(11):644–659, 2020.

B. A. Riedner, B. K. Hulse, M. J. Murphy, F. Ferrarelli, and G. Tononi. Temporal dynamics of cortical sources underlying spontaneous and peripherally evoked slow waves. *Progress in brain research*, 193:201–218, 2011.

T. Roenneberg, A. Wirz-Justice, and M. Merrow. Life between clocks: daily temporal patterns of human chronotypes. *Journal of biological rhythms*, 18(1):80–90, 2003.

T. Rosinvil, J. Bouvier, J. Dubé, A. Lafrenière, M. Bouchard, J. Cyr-Cronier, N. Gosselin, J. Carrier, and J.-M. Lina. Are age and sex effects on sleep slow waves only a matter of electroencephalogram amplitude? *Sleep*, 44(3):zsaa186, 2021.

S. Ruch, F. J. Schmidig, L. Knüsel, and K. Henke. Closed-loop modulation of local slow oscillations in human nrem sleep. *NeuroImage*, 264:119682, 2022.

Y. Sato, Y. Fukuoka, H. Minamitani, and K. Honda. Sensory stimulation triggers spindles during sleep stage 2. *Sleep*, 30(4):511–518, 2007.

M. Schabus, G. Gruber, S. Parapatics, C. Sauter, G. Klösch, P. Anderer, W. Klimesch, B. Saletu, and J. Zeitlhofer. Sleep spindles and their significance for declarative memory consolidation. *Sleep*, 27 (8):1479–1485, 2004.

J. Schneider, P. A. Lewis, D. Koester, J. Born, and H.-V. V. Ngo. Susceptibility to auditory closed-loop stimulation of sleep slow oscillations changes with age. *Sleep*, 43(12):zsaa111, 2020.

P. L. Smith and D. R. Little. Small is beautiful: In defense of the small-n design. *Psychonomic bulletin & review*, 25(6):2083–2101, 2018.

F. Tadel, S. Baillet, J. C. Mosher, D. Pantazis, and R. M. Leahy. Brainstorm: a user-friendly application for meg/eeg analysis. *Computational intelligence and neuroscience*, 2011, 2011.

C. Tesche, M. Uusitalo, R. Ilmoniemi, M. Huotilainen, M. Kajola, and O. Salonen. Signal-space projections of meg data characterize both distributed and well-localized neuronal sources. *Electroencephalography and clinical neurophysiology*, 95(3):189–200, 1995.

D. Thissen, L. Steinberg, and D. Kuang. Quick and easy implementation of the benjamini-hochberg procedure for controlling the false positive rate in multiple comparisons. *Journal of educational and behavioral statistics*, 27(1):77–83, 2002.

I. Timofeev and S. Chauvette. Sleep slow oscillation and plasticity. *Current opinion in neurobiology*, 44:116–126, 2017.

N. Valenchon, Y. Bouteiller, H. R. Jourde, X. L'Heureux, M. Sobral, E. B. Coffey, and G. Beltrame. The portiloop: A deep learning-based open science tool for closed-loop brain stimulation. *PloS one*, 17 (8):e0270696, 2022.

V. V. Vyazovskiy and K. D. Harris. Sleep and the single neuron: the role of global slow oscillations in individual cell rest. *Nature Reviews Neuroscience*, 14(6):443–451, 2013.

E. F. Wijdicks. The ascending reticular activating system. *Neurocritical Care*, 31(2):419–422, 2019.

M. Wunderlin, M. A. Züst, E. Hertenstein, K. D. Fehér, C. L. Schneider, S. Klöppel, and C. Nissen. Modulating overnight memory consolidation by acoustic stimulation during slow-wave sleep: A systematic review and meta-analysis. *Sleep*, 44(7):zsaa296, 2021.

S. S. Yeo, P. H. Chang, and S. H. Jang. The ascending reticular activating system from pontine reticular formation to the thalamus in the human brain. *Frontiers in human neuroscience*, 7:416, 2013.

U. Ziemann and H. R. Siebner. Inter-subject and inter-session variability of plasticity induction by non-invasive brain stimulation: boon or bane? *Brain Stimulation: Basic, Translational, and Clinical Research in Neuromodulation*, 8(3):662–663, 2015.